General Disclaimer

One or more of the Following Statements may affect this Document

- This document has been reproduced from the best copy furnished by the organizational source. It is being released in the interest of making available as much information as possible.

- This document may contain data, which exceeds the sheet parameters. It was furnished in this condition by the organizational source and is the best copy available.

- This document may contain tone-on-tone or color graphs, charts and/or pictures, which have been reproduced in black and white.

- This document is paginated as submitted by the original source.

- Portions of this document are not fully legible due to the historical nature of some of the material. However, it is the best reproduction available from the original submission.

MULTIPLE BUOYANCY DRIVEN FLOWS IN A

VERTICAL CYLINDER HEATED FROM BELOW

by

Y. Yamaguchi, C.J. Chang, and R.A. Brown

Department of Chemical Engineering
Massachusetts Institute of Technology
Cambridge, MA   02139

February   1983

ABSTRACT

The structure of axisymmetric buoyancy-driven convection in a vertical cylinder heated from below is probed by finite element solution of the Boussinesq equations coupled with computed-implemented perturbation techniques for detecting and tracking multiple flows and for determining flow stability. Results are reported for fluids with Prandtl number of one and for cylinders with aspect ratio Λ (defined as the height to radius of the cylinder) between 0.5 and 2.25. Extensive calculations of the neutral stability curve for the static solution and of the nonlinear motions along the bifurcating flow families show a continuous evolution of the primary cellular motion from a single toroidal cell to two and three cells nested radially in the cylinder, instead of the sharp transitions found for a cylinder with shear-free sidewalls. The smooth transitions in flow structure with Rayleigh number and Λ are explained by nonlinear connectivity between the first two bifurcating flow families formed either by a secondary bifurcation point for $\Lambda \leq \Lambda^* \simeq 0.80$ or by a limit point for $\Lambda \geq \Lambda^*$. The transition between these two modes may be described by the theory of multiple limit point bifurcation.

CONTENTS

1. INTRODUCTION

Since the early works of Bénard (1901) and Rayleigh (1916) for a horizontal fluid layer, the onset and evolution of convective motions caused by temperature-induced buoyancy differences have been the focus of extensive theoretical and experimental research. For geometries with imposed temperature fields that are purely vertical and heated from below, convection begins at a critical temperature difference, measured in terms of the Rayleigh number, beyond which the static fluid is unstable to small amplitude disturbances of the velocity, pressure and temperature fields. These critical Rayleigh numbers are determined as the eigenvalues for marginal stability in an analysis constructed from the Boussinesq equations linearized about the static state.

The calculation of the fluid motions that evolve for Rayleigh numbers away from the critical values requires nonlinear analysis, either by perturbation methods (Schlüter et al. 1965) or by numerical solution of the full Boussinesq equations. Perturbation methods are only feasible for geometries where at least part of the boundary is shear-free and eigenfunctions for the field variables can be written in terms of only a few special functions. Even in these systems limitations on the range of validity of the perturbation technique confine the results to flows only slightly perturbed from the rest state. Numerical calculations have the potential for determining these flows over a much wider range of Rayleigh number and describing the nonlinear evolution of the structure with changes in the geometry of the cavity and Prandtl number. The purpose of this paper is to describe such a numerical study for axisymmetric convection in a vertical cylinder heated from below.

We report calculations for the form and stability of the steady two-dimensional flows in a cylinder with rigid boundaries and insulated sidewall. These flows are computed by combining finite-element methods for solving the

Boussinesq equations with efficient computer-aided schemes for tracking the evolution and multiplicity of the flow field with changes in parameters, such as Rayleigh number.

The numerical techniques for calculating solution multiplicity and stability have been developed as outgrowths of classical asymptotic analysis of bifurcation in systems of algebraic equations (cf. Keller 1977; Brown and Scriven, 1980a; Ungar and Brown 1982) and are applied here to the finite-dimensional equation set that results from the finite-element approximation to the Boussinesq equations. With this approach, we are able to extend previous calculations for the flows evolving from rest while simultaneously determining nonlinear interactions between families of flows. The stability results presented here are based on a linear analysis of the stability of the finite-element solutions to small perturbations in the field variables and are computed by schemes that make use of the connections between the change of stability of a family of flows and the occurence of a critical value of Rayleigh where the flow is locally not unique. These techniques are general for all disturbances, except those leading to time-periodic bifurcation, and are much more efficient than the eigenvalue calculations used in previous studies (Brown and Scriven 1980a; 1980b).

The cataloging of the branching and evolution of multiple flow fields is a fruitful approach to the description of nonlinear natural convection and the effect of varying parameters and geometry, as has been recently demonstrated by the studies of Daniels (1977 & 1979), Tavantis et al. (1978), and Hall and Walton (1977 & 1979). In this framework, the critical Rayleigh numbers $\{Ra_c^{(i)}\}$ determined from linear stability analysis mark the points of bifurcation between families of flows and the rest state; the eigenfunctions describe the structure of the new flows near the respective bifurcation points. A simple eigenvalue

- 3 -

$Ra_c^{(i)}$ along the static family is then a simple bifurcation point joining
two flow families, the static one and the new family of flows. These flows
exist for some range of Rayleigh number beyond the $Ra_c^{(i)}$, as shown by asymp-
totic analyses for rectangular cavities (Schlüter et al. 1965; Daniel 1977;
Hall and Walton 1977) and for a cylinder with shear-free boundaries (Liang
et al. 1969; Rosenblat 1982). The critical values $\{Ra_c^{(i)}\}$ have been obtained
for vertical cylinders with several combinations of rigid and shear-free
boundaries.

Zierep (1959) first calculated these for a cylinder with rigid ends and
shear-free sidewall and found that particular cellular flow structures were
associated uniquely with each critical Rayleigh number. The ordering of the
set $\{Ra_c^{(i)}\}$ depended on the aspect ratio (defined as the radius over the
height). Distinct values of Λ existed where two critical values of Ra were
equal and where two flow patterns were equally likely. These values of Ray-
leigh number are double bifurcation points (Iooss and Joseph 1980) in the full
nonlinear problem and, as shown by Bauer et al. (1975), signal the possibility
of secondary bifurcation along one of the new flow families for aspect ratios
just slightly perturbed from this special value. Hall and Walton (1979) noted
the existence of double points for the onset of convection in a rectangular
cavity with rigid sidewalls and shear-free ends and used amplitude expansions
to show the existence of a secondary bifurcation point. Double points are
most simply found for a cylinder with shear-free boundaries all around (Liang
et al. 1969), as demonstrated by the plot of $\{Ra_c^{(i)}\}$ for axisymmetric modes of
convection as a function of aspect ratio shown as Figure 1. Recently, Rosenblat
(1982) has used approximations formed from truncated eigenfunction expansions to
find secondary steady bifurcation of families of steady flows near double
points between axisymmetric and non-axisymmetric modes for a cylinder with
totally shear-free walls.

The boundary conditions on velocity at the sidewall of the cylinder have a striking effect on the evolution of the critical values with aspect ratio and thus on the existence of the double points and secondary bifurcation. As is shown below, a cylinder with rigid walls exhibits no crossing of the first and second critical Rayleigh numbers for aspect ratios between 0.5 and 2.75. Instead, the cellular structure of the flow branching from $Ra_c^{(1)}$ changes continuously with varying Λ. This result is in agreement with the velocity profiles shown by Charlson and Sani (1970) for the onset of convection in the same problem and for calculations from an approximate analysis Brown and Stewartson (1978) valid for large aspect ratios in a cylinder with rigid sidewall and shear-free ends. This latter linear analysis formed the basis of nonlinear studies (Brown and Stewartson 1978 & 1979) of the effect on the structure of the bifurcating flow family of the sidewall and imperfections in the insulating condition along it. Exact calculations of the critical Rayleigh numbers for a cylinder with shear-free ends were reported by Joseph (1971), but insufficient information about the velocity component of the eigenfunction was given to deduce the evolution of the flow structure with Λ.

Numerical calculations of the finite amplitude flows in a vertical cylinder have been performed with the three combinations of shear-free and no-slip boundary conditions mentioned above. Liang et al. (1969) list sixteen finite difference calculations, all near the critical Rayleigh number, for different combinations of boundary conditions and including the dependence of viscosity on temperature. Jones et al. (1976) used time-dependent finite difference techniques to calculate the flow patterns in a cylinder with shear-free boundaries for Rayleigh numbers up to 100 Ra_c and Prandtl numbers, ranging between 0.1 and the limiting case of infinity. They found a continuous family of flow fields that developed over this range of Ra with no qualitative change in the structure of the flow from the single toroidal cell predicted from the eigenfunction at $Ra=Ra_c^{(1)}$. Charlson and

Sani (1975) have used approximations in terms of eigenfunctions to compute the finite amplitude flows and stability for a cylinder with all rigid boundaries, the configuration treated here. They present results for several aspect ratios and Prandtl numbers for Ra up to three times the critical value.

The outline of the paper is as follows. The formulation of the natural convection problem is presented in §2 and the finite element approximation and numerical techniques for tracking solution families are reviewed in §3. The links between bifurcations in the families of steady flows and the stability of each flow are established in §4 and the criteria for exchanges of stability are presented. Results of calculations of the onset of convection and the evolution of the flow families are represented in §5-7 .

- 6 -

2. FORMULATION

We study the axisymmetric two-dimensional flows in a rigid vertical cylinder of height L and radius R filled with a fluid that has constant thermal diffusivity α and kinematic viscosity ν. The two ends are taken to be isothermal with the lower one held at a temperature ΔT above the temperature T_c of the upper surface. Two different thermal conditions are examined for the cylindrical sidewall; either it is assumed to be a perfect insulator or it is taken as a perfect conductor so that a linear temperature profile exists along this wall connecting the temperatures at the top and bottom ends. Both conditions were studied in Charlson and Sani (1970 and 1975) and the later case is included here for comparison to their calculations.

The dimensionless forms of the Boussinesq equations that govern the temperature $\theta(r,z,t)$, pressure $p(r,z,t)$ and velocity $\underline{v}(r,z,t)$ fields are

$$\nabla \cdot \underline{v} = 0 \tag{2.1}$$

$$\frac{\partial \underline{v}}{\partial t} + \underline{v} \cdot \nabla \underline{v} = -\nabla p + Pr\nabla^2 \underline{v} + RaPr\,\theta\,\underline{e}_z , \tag{2.2}$$

$$\frac{\partial \theta}{\partial t} + \underline{v} \cdot \nabla \theta = \nabla^2 \theta , \tag{2.3}$$

where ∇ is the gradient operator in cylindrical coordinates and $\underline{e}_z$ is the unit vector in the vertical direction. The variables $(\underline{v},p,\theta)$ have been put in dimensionless form by scaling lengths with the height of the cylinder L, velocity with α/L, pressure with $\rho\alpha^2/L^2$, time with L^2/α and temperature as $(T(r,z,t)-T_c)/\Delta T$, where $T(r,z,t)$ is the dimensional temperature field and ρ is the density of the fluid. The Rayleigh and Prandtl numbers appear in eqs. (2.1-2.3) and are defined as

$$Ra = \beta g L^3 \Delta T / \alpha \nu \qquad , \quad Pr = \nu/\alpha \quad , \qquad (2.4)$$

where β and g are the coefficient of thermal expansion and acceleration of gravity, respectively.

The boundary conditions for the velocity field are

$$v_r = v_z = 0 \quad , \qquad 0 \leq r \leq \Lambda \quad , \qquad z = 0,1 \qquad , \qquad (2.5)$$

$$v_r = v_z = 0 \quad , \qquad r = \Lambda \quad , \qquad 0 \leq z \leq 1 \qquad , \qquad (2.6)$$

$$v_r = \partial v_z / \partial r = 0 \quad , \qquad r = 0 \quad , \qquad 0 \leq z \leq 1 \qquad , \qquad (2.7)$$

where $\Lambda \equiv R/L$ is the aspect ratio. When the sidewall is insulated the boundary conditions on temperature are

$$\theta = 0 \qquad\qquad 0 \leq r \leq \Lambda \quad , \qquad z = 1 \quad , \qquad (2.8)$$

$$\theta = 1 \qquad\qquad 0 \leq r \leq \Lambda \quad , \qquad z = 0 \quad , \qquad (2.9)$$

$$\partial\theta / \partial r = 0 \qquad\quad r = 0 \quad , \qquad 0 \leq z \leq 1 \quad . \qquad (2.10)$$

The thermal boundary conditions for a cylinder with a perfectly conducting sidewall are the same as eqs. (2.8-2.10), except the condition evaluated at $r = \Lambda$, eq. (2.10), is replaced by

$$\theta = 1-z \qquad , \qquad r = \Lambda \quad , \qquad 0 \leq z \leq 1 \quad . \qquad (2.11)$$

For either set of thermal conditions the entire equation set has the static solution

$$\underline{v} = \underline{0} \quad , \qquad \theta = 1-z \quad , \quad p = p_0 + RaPr(z-z^2/2) \quad , \qquad (2.12)$$

from which the convective motions branch. We will represent these flows by Nusselt numbers defined as

$$Nu = \frac{2}{R^2} \int_0^\Lambda \frac{\partial \theta}{\partial z} \; r \; dr \quad , \tag{2.13}$$

where the temperature gradient is evaluated along either the top (N_u^T) or bottom (N_u^B) ends of the cylinder.

- 9 -

3. NUMERICAL METHODS

3.1 Calculation of Steady Flows

Finite element methods are well established for solving the steady and transient Boussinesq equations and boundary conditions. We use a method for mixed-order polynomial interpolation of velocities, temperature, and pressure that has been proposed before (see Zienkiewicz et al. 1976, Huyakorn et al. 1979, Taylor and Ijam 1979). The fluid domain ($0 \leq r \leq \Lambda$, $0 \leq z \leq 1$) is first divided into equally spaced quadrilateral elements. On this discretization, the components of velocity and the temperature are approximated by expansions in terms of biquadratic polynomials $\{\phi^j(r,z)\}$ as

$$\begin{bmatrix} v_r(r,z,t) \\ v_z(r,z,t) \\ \theta(r,z,t) \end{bmatrix} = \sum_{j=1}^{N_i} \begin{bmatrix} u_j(t) \\ v_j(t) \\ \theta_j(t) \end{bmatrix} \phi^i(r,z) + \sum_{j=1}^{N_e} \begin{bmatrix} u_j^e \\ v_j^s \\ \theta_j^e \end{bmatrix} \phi^j(r,z) + \sum_{j=1}^{N_s} \begin{bmatrix} u_j^s \\ v_j^s \\ \theta_j^s(t) \end{bmatrix} \phi^j(r,z) ,$$

(3.1)

where the limits on the summations represent types of nodes in the elemental discretization; N_i is the number of nodes in the interior of the domain, N_e represents the nodes along the top and bottom ends of the cylinder, and N_s is the number of nodes along the sidewall. Each biquadratic function $\phi^j(r,z)$ is defined to have a value of one at the node with which it is associated and to be zero at all other nodes. Because of this definition, the coefficients $(u_j(t), v_j(t), \theta_j(t))$ represent the values of the field variables at the locations of the nodes. The boundary conditions on temperature and velocity specify many of these coefficients and reduce the number of unknowns that must be computed, with the exact number depending on the choice of thermal boundary condition. The remainder of the analysis is presented for the case of the sidewall being insulated. Then eqs. (2.8-2.10) set the coefficients $\{u_j^e, v_j^e, \theta_j^e\}$, $j=1, \ldots N_e$

and $\{u_j^s, v_j^s\}$, $j=1, \ldots N_s$.

The pressure is approximated by the expansion in terms of bilinear polynomials $\{\psi^j(r,z)\}$ as

$$p(r,z,t,) = \sum_{j=1}^{M} p_j(t)\psi^j(r,z) , \qquad (3.2)$$

where M is the number of vertex nodes in the finite element mesh. Each function $\psi^j(r,z)$ is defined so that it has a value of one at the jth vertex node and is zero at all others. More details of both sets of basis functions are available in many references (e.g. Thomasset 1981).

The weak forms of the field equations are formed by applying Galerkin's method to eqs. (2.1-2.3). Each field equation is weighted with the basis function corresponding to the finite element expansion for the appropriate field variable and is integrated over the fluid domain:

$$\frac{\partial}{\partial t} \int_D \phi^i \underline{v} \cdot \underline{e}_k \, dA = - \int_D \phi^i [\underline{e}_k \cdot \underline{v} \cdot \nabla \underline{v} + \underline{e}_k \cdot \nabla p - Pr\underline{e}_k \cdot \nabla^2 \underline{v} - RaPr\theta(\underline{e}_z \cdot \underline{e}_k)] \, dA$$

$$, k=r,z \quad , i=1, \ldots N_i \qquad (3.3)$$

$$\frac{\partial}{\partial t} \int_D \phi^i \theta \, dA = \int_D \phi^i [\nabla^2 \theta - \underline{v} \cdot \nabla \theta] \, dA \quad , i=1 , \ldots N_i + N_s \qquad (3.4)$$

$$0 = \int_D \psi \nabla \cdot \underline{v} \, dA \quad , i=1, \ldots M . \qquad (3.5)$$

The final forms of the residual equations are derived by applying the divergence-theorem to eqs. (3.3, 3.4), by substituting in the expansions (3.1, 3.2), and by incorporating the boundary conditions for temperature and velocity. After these simplifications, the residual equations are reduced to the nonlinear ordinary differential equations

$$\sum_{j=1}^{N_i} \frac{du_j}{dt} \int_{\mathcal{D}} \phi^i \phi^j \, dA = \int_{\mathcal{D}} \left\{ \phi^i \left(-v_r \frac{\partial v_r}{\partial r} - v_z \frac{\partial v_r}{\partial z} - \frac{\partial p}{\partial r} - Pr \frac{1}{r} \frac{\partial v_r}{\partial r} \right) \right.$$

$$\left. - Pr \left(\frac{\partial \phi^i}{\partial r} \frac{\partial v_r}{\partial r} - \frac{\partial \phi^i}{\partial z} \frac{\partial v_r}{\partial z} \right) \right\} dA \ , \quad i=1, \cdots N_i \ , \quad (3.6)$$

$$\sum_{j=1}^{N_i} \frac{dv_j}{dt} \int_{\mathcal{D}} \phi^i \phi^j \, dA = \int_{\mathcal{D}} \left\{ \phi^i \left(-v_r \frac{\partial v_z}{\partial r} - v_z \frac{\partial v_z}{\partial z} - \frac{\partial p}{\partial z} - Pr \frac{1}{r} \frac{\partial v_z}{\partial r} - Ra Pr \, \theta \right) \right.$$

$$\left. - Pr \left(\frac{\partial \phi^i}{\partial r} \frac{\partial v_z}{\partial r} + \frac{\partial \phi^i}{\partial z} \frac{\partial v_z}{\partial z} \right) \right\} dA \ , \quad i=1, \ldots N_i \ , \quad (3.7)$$

$$\sum_{j=1}^{N_i + N_s} \frac{d\theta_j}{dt} \int_{\mathcal{D}} \phi^i \phi^j \, dA = \int_{\mathcal{D}} \left\{ \phi^i \left(-v_r \frac{\partial \theta}{\partial r} - v_z \frac{\partial \theta}{\partial z} \right) - \frac{\partial \phi^i}{\partial r} \frac{\partial \theta}{\partial r} - \frac{\partial \phi^i}{\partial z} \frac{\partial \theta}{\partial z} \right\} dA \ ,$$

$$i=1, \ldots N_i + N_s \ , \quad (3.8)$$

$$0 = \int \psi^j \left(\frac{1}{r} \frac{\partial}{\partial r}(r v_r) + \frac{\partial v_z}{\partial z} \right) dA = 0 \quad , \ i=1, \ldots M \ . \quad (3.9)$$

This set is compactly represented by the notation

$$\underline{\underline{M}} \frac{dx}{dt} = \underline{R}(\underline{x}; Ra, \ Pr, \Lambda) \ , \quad (3.10)$$

where $\underline{x}$ is the vector of unknown coefficients

$$\underline{x}^T \equiv (u_1, u_2, \ldots u_{N_i}, v_1, v_2, \ldots v_{N_i}, \ \theta_1, \ \theta_2, \ \ldots \theta_{N_i + N_s}, p_1, p_2, \ldots p_M) \ , \quad (3.11)$$

and the vector $\underline{R}$ represents the nonlinear algebraic equations that compose the right hand sides of eqs. (3.5-3.8). The mass matrix $\underline{\underline{M}}$ is sparse and has components that are integrals of products of basis functions, but is mathema-

tically singular because of the absence of time derivatives from the continuity equation.

Steady state solutions of the natural convection problem are found by solving the $N_t \equiv (3N_i + N_s + M)$ equations

$$\underline{R}(x;Ra) = \underline{0} \quad , \tag{3.12}$$

for given values of the parameters. We calculate families of solutions to eq. (3.11) by combining Newton's iteration with continuation methods (Kubieck 1976) for approximating the sensitivity of the solution vector $\underline{x}$ on Rayleigh number. The details of these methods are laid out in Ungar and Brown (1982) and only points important to the developments in §4 are included here.

Starting from a first approximation to the solution vector $\underline{x}^{(0)}$, Newton's method forms iterates as

$$\underline{x}^{(i+1)} = \underline{x}^{(i)} - \underline{\delta}^{(i+1)} \equiv \underline{x}^{(i)} - \underline{\underline{J}}^{-1}(\underline{x}^{(i)})\underline{R}(\underline{x}^{(i)}; Ra) \quad , \tag{3.13}$$

where $\underline{\underline{J}}$ is the Jacobian matrix of the equation set (3.12), i.e. $J_{ij} \equiv \partial R_i/\partial x_j$. The Jacobian matrix is asymmetric and has nonzeroes banded about the main diagonal because of the limited overlap of the finite element basis functions. The system of linear equations

$$\underline{\underline{J}}\,\underline{\delta}^{(i+1)} = -\underline{R}(\underline{x}^{(i)};Ra) \tag{3.14}$$

is solved by Gaussian elimination with diagonal pivoting using the frontal routine of Hood (1976) to minimize the amount of computer memory necessary to perform the calculations.

The first guess of the solution vector for a Rayleigh number $Ra^o + \Delta Ra$ different from Ra^o, where $\underline{x}(Ra^o)$ has been calculated before, is approximated as

$$\underline{x}^{(0)}(Ra_0 + \Delta Ra, Pr, \Lambda) = \underline{x}(Ra_0, Pr, \Lambda) + \underline{x}_{Ra} \cdot \Delta Ra \quad , \tag{3.15}$$

where the tangent vector $\underline{x}_{Ra}$ is calculated from the linear set that results from taking the directional derivative of eqs. (3.12) along the solution family

$$\underline{J}(Ra_0, Pr, \Lambda)\underline{x}_{Ra} = -(\partial \underline{R}/\partial Ra)_{Ra_0} \quad , \tag{3.16}$$

which is solved simultaneously with the last Newton iteration.

3.2 Calculation of Limit Points, Bifurcation Points and Multiple Flow Fields

Continuous families of flow fields are calculated by combining Newton iterations with continuation methods as long as the flows are uniquely specified by Ra and no bifurcations to other families occur. The non-uniqueness with respect to Ra in a single family appears near a limit point Ra_ℓ where the family reverses direction in Ra. Classical perturbation methods are well known for analyzing both limit and bifurcation points and have been adapted by several researchers (Keller 1977, Rheinboldt 1978, Brown et al. 1980) for implementation in numerical algorithms; the methods used here follow techniques developed by Keller (1977).

Calculations near bifurcation and limit points are performed effectively by introducing an amplitude parameter ε defined so that each family of flows is uniquely specified as $(\underline{x}(\varepsilon), Ra(\varepsilon))$ in the neighborhood of the singular point fixed at $\varepsilon = 0$. Following perturbation methods used in classical bifurcation analysis, the solution vector $\underline{x}$ and parameter Ra are expanded as

$$\begin{bmatrix} x(\varepsilon) \\ Ra(\varepsilon) \end{bmatrix} = \sum_{k=0}^{\infty} \frac{\varepsilon^k}{k!} \begin{bmatrix} \underline{x}_{(k)} \\ Ra_{(k)} \end{bmatrix} \quad , \tag{3.17}$$

where the components $(\underline{x}_{(k)}, Ra_{(k)})$ are determined from the nonlinear equation set (3.12) expanded to the appropriate order of ε . The sets governing the corrections $(\underline{x}_{(1)}, Ra_{(1)})$ and $(\underline{x}_{(2)}, Ra_{(2)})$ are

$$\underline{R}_x(\underline{x}(0); Ra(0))\underline{x}_{(1)} = -\underline{R}_{Ra}(\underline{x}(0); Ra(0))Ra_{(1)} \quad , \tag{3.18}$$

$$\underline{R}_x(\underline{x}(0); Ra(0))\underline{x}_{(2)} = -\underline{R}_{xx}\underline{x}_{(1)}\underline{x}_{(1)} - 2\underline{R}_{xRa}(\underline{x}(0); Ra(0))\underline{x}_{(1)}\underline{Ra}_{(1)}$$
$$-\underline{R}_{Ra}(\underline{x}(0); Ra(0))Ra_{(2)} - \underline{R}_{RaRa}Ra_{(1)}^2 \quad . \tag{3.19}$$

In eq. (3.19), $\underline{R}_{xx}$ is the $(N_t \times N_t \times N_t)$-dimensional matrix with components $\{\underline{R}_{xx}\}_{ijk} \equiv \partial R^i / \partial x_j \partial x_k$; $\underline{R}_{xRa}$ is the $(N_t \times N_t)$-dimensional matrix with $\{R_{xRa}\}_{ij} \equiv \partial R^i / \partial x_j \partial Ra$; and $\underline{R}_{RaRa}$ is the vector with $\{\underline{R}_{RaRa}\}_i \equiv \partial^2 R^i / \partial Ra^2$. This last vector is zero for the Bousinesq equations. The $(N_t \times N_t)$-dimensional matrix $\underline{R}_x$ appearing in eq. (3.18) and (3.19) is identical to the Jacobian matrix evaluated about the solution at the singular point. Terms in the expansion (3.17) can be computed once a suitable definition of ε is selected; different definitions are used here for handling bifurcation and limit points.

Riks (1972) first introduced and Keller (1977) refined the idea of introducing the pseudo arc-length s for yielding local representations of the members of a solution family, even in the neighborhood of a limit point, and this is a suitable definition of the amplitude parameter ε , that is $\varepsilon \equiv s - s_0$. For computing around limit points, we introduce the arc-length evaluated from the known solution $(\underline{x}(s_0) , Ra(s_0))$ through an additional residual equation

$$R_{N_{t+1}} \equiv (s-s_0)^2 + ||\underline{x}(s) - \underline{x}(s_0)||_2^2 + |Ra(s)-Ra(s_0)|^2 \quad , \tag{3.20}$$

where $||\underline{x}||_2$ is the R_2-norm of $\underline{x}$, i.e. $||\underline{x}||_2^2 = \sum_{i=1}^{N_t} x_i^2$. The tangent vector $(\underline{x}_{(1)}, Ra_{(1)})$ for implementing continuation is computed by solving eq. (3.18)

augmented with the linearization of eq. (3.20) about the known solution

$$(s-s_0) + \underline{d}^T \underline{x}_{(1)} + (Ra(s) - Ra(s_0)) = 0 \quad , \qquad (3.21)$$

where $d_i \equiv \partial R_{N_t+1}/\partial x_i$. The (N_t+1)-dimensional matrix formed from eqs.
(3.18) and (3.21) is nonsingular at limit points (Keller 1977) and so the
nonlinear set (3.12) augmented with eq. (3.20) is solved by Newton's method.
The limiting value of Rayleigh number $Ra_\ell \equiv Ra(s_\ell)$ is determined from the
criterion $Ra_{(1)} \equiv (dRa/ds)_{s_\ell} = 0$. At $Ra = Ra_\ell$ the right hand side of eq.
(3.18) vanishes and $\underline{x}_{(1)}$ is determined as the solution of the homogeneous
set and the orthogonalization condition (3.21); the solution of this problem
is discussed in the next section.

At values of Ra for bifurcation the Jacobian matrix is singular and the
tangent vector $\underline{x}_{Ra}$ has multiple values. For simple bifurcation points only
one eigenvalue of $\underline{\underline{J}}$ passes through zero and bifurcation is detected by moni-
toring the sign of the determinant of $\underline{\underline{J}}$. The null vector $\underline{z}$ corresponding to
the zero eigenvalue and its adjoint vector $\underline{y}$ satisfy

$$\underline{\underline{J}}(\underline{x}(Ra_c); Ra_c)\underline{z} = 0 \; , \; \underline{\underline{J}}^T(\underline{x}(Ra_c); Ra_c)\underline{y} = 0 \; , \; \underline{z}^T\underline{y} = 1 \; , \qquad (3.22)$$

where $\underline{\underline{J}}^T$ is the transpose of $\underline{\underline{J}}$ and is also banded. The null vectors are
calculated by Gaussian elimination with partial pivoting as implemented in
the frontal routine. The singularity of $\underline{\underline{J}}$ and the non-uniqueness of the null
vectors are accounted for by ignoring the last row in the upper triangular
matrix and by setting the N_t-th element of $\underline{z}$ and $\underline{y}$ to unity; these vectors
are later normalized so that $\|\underline{z}\|_2 = \|\underline{y}\|_2 = 1$.

The continuation vector $\underline{x}_{(1)}$ written in terms of ε , is decomposed at

$Ra = Ra_c$ into components in the null space and range of $\underline{\underline{J}}$ as

$$\underline{x}_{(1)} \equiv \underline{z}_0 + A\underline{z} \quad , \tag{3.23}$$

where $\underline{z}$ is the null vector, A is an as-yet undetermined constant and $\underline{z}_0$ is the particular solution of eq. (3.18) that contains no component of $\underline{z}$, i.e. that satisfies $\underline{y}^T \underline{z}_0 = 0$. Because the right hand side of (3.18) is homogeneous in $Ra_{(1)}$, $\underline{z}_0 \equiv Ra_{(1)}\underline{c}$ where $\underline{c}$ is the particular solution of

$$\underline{\underline{J}}(\underline{x}(Ra_c); Ra_c)\underline{c} = -\underline{R}_{Ra}(\underline{x}(Ra_c); Ra_c) \quad , \tag{3.24}$$

that is orthogonal to $\underline{y}$. Equation (3.25) is solvable only if

$$\underline{y}^T \underline{R}_{Ra}(\underline{x}(Ra)_c; Ra_c) = 0 \quad , \tag{3.25}$$

that is, the vector $\underline{R}_{Ra}$ must be in the range of $\underline{\underline{J}}$. Bifurcation between the two solution families is guaranteed when Ra_c is a simple eigenvalue and eq. (3.25) is satisfied (see Keller 1977 and Iooss and Joseph 1980).

The tangent vectors to the base and bifurcating solution families are determined from (3.23) after A and $Ra_{(1)}$ are computed from the definition of ε and the solvability condition for the second-order problem (3.19). For analyzing simple bifurcation points in a flow family $(\hat{\underline{x}}(\varepsilon), \hat{\mu}(\varepsilon))$ we use the amplitude definition

$$\varepsilon \equiv A\underline{y}^T(\underline{x}(\varepsilon) - \hat{\underline{x}}(0)) + Ra_{(1)}(Ra(\varepsilon) - \hat{Ra}(0)) \quad , \tag{3.26}$$

where A and $\mu_{(1)}$ are associated with the solution family along which ε is being defined. At first order in ε eq. (3.26) requires that

$$1 = A^2 + Ra_{(1)}^2 \quad . \tag{3.27}$$

The solvability condition for the second-order problem is

$$A^2 C_1 + 2A Ra_{(1)} C_2 + Ra_{(1)}^2 C_3 = 0 \quad , \tag{3.28}$$

where

$$
\begin{aligned}
C_1 &\equiv \underline{y}^T \underline{R}_{xx} \underline{z}\underline{z} \quad , \\[6pt]
C_2 &\equiv \underline{y}^T \underline{R}_{xx} \underline{c}\underline{z} + \underline{y}^T \underline{R}_{xRa} \underline{z} \quad , \\[6pt]
C_3 &\equiv 2\underline{y}^T \underline{R}_{xRa} \underline{c} + \underline{y}^T \underline{R}_{xx} \underline{c}\underline{c} \quad ,
\end{aligned}
\right\} \tag{3.29}
$$

where the arguements of the derivatives of $\underline{R}$ are the same as in (3.19). Equations (3.27) and (3.28) are the same bifurcation equations derived by Keller (1977). The two pairs $(A, Ra_{(1)})$ are calculated as roots of these equations once the coefficients $\{C_i\}$ are determined at the bifurcation point $Ra = Ra_c$. We approximate derivatives of the form $\underline{R}_{xx}\underline{a}\underline{b}$ using the difference formula

$$\underline{y}^T \underline{R}_{xx}(\underline{x}(0); Ra(0))\underline{a}\underline{b} \simeq \underline{y}^T [\underline{R}_x(\underline{x}(0) + \delta\underline{a}; Ra(0)) - \underline{R}_x(\underline{x}(0); Ra(0))]\underline{b}/\delta \quad , \tag{3.30}$$

where δ is a small positive constant, taken here as 10^{-3}. The matrix $\underline{R}_{xRa}$ is calculated exactly.

Flows in the bifurcating families are calculated by Newton iteration with an initial approximation given by eq. (3.17). The amplitude ε is picked to be large enough that the iterations converge to a flow in the new family. When $Ra_{(1)}$ is zero the new family evolves either super- or sub-critically and we search values of Ra both above and below Ra_c for new flows using first approximations composed entirely of the null space. Either super- or sub-critical bifurcation ($Ra_{(1)} = 0$) occurs when $C_1 = 0$; see eq. (3.28).

4. BIFURCATION AND STABILITY

The relative stability of flows in individual families to small perturbations of the velocity, temperature, and pressure fields can change only at bifurcation and limit points in families of steady flows and at Hopf bifurcation points that mark the beginning of time-periodic motions. The discretized form of the Boussinesq equations (3.10) is a convenient framework for developing simple criteria for accessing the exchange of stability at the steady bifurcation and limit points detected by methods outlined in §3.2 . In this Section, we use ideas presented by Iooss and Joseph (1980) to extend earlier stability results developed by Szeto (1978).

The stability of a steady flow $(\hat{\underline{x}}(Ra), Ra)$ is analyzed with respect to small perturbations to the field variables represented in the same finite element bases presented in §3.1 as

$$\underline{x}(t;Ra) = \hat{\underline{x}}(Ra) + \underline{u}(t) = \hat{\underline{x}}(Ra) + \hat{\underline{u}}e^{\sigma t} \quad , \tag{4.1}$$

where the vector $\hat{\underline{u}}$ is independent of time. Linearizing eq. (3.10) for the evolution of a vector described by (4.1) gives the generalized eigenvalue problem for stability

$$\sigma \underline{\underline{M}}\hat{\underline{u}} = \underline{\underline{R}}_x(\hat{\underline{x}}(Ra) ; Ra)\hat{\underline{u}} \quad , \tag{4.2}$$

where $\underline{\underline{R}}_x(\hat{\underline{x}}(Ra); Ra)$ is the Jacobian matrix of $\underline{R}$ evaluated about the steady solution. The stability of this flow can be completely determined by computing the eigenvalues of eq. (4.2); however, repeated eigenvalue calculations are not feasible for the large matrices that result from the finite-element approximations. Instead, we develop stability criteria for the case when an eigenvalue σ is zero at $Ra = Ra_c$ and passes through zero as Ra is varied past Ra_c along the primary

flow family. The criteria focus on determining the sign of the derivative $(d\sigma/dRa)$ at Ra = Ra_c .

The adjoint eigenvalue problem to (4.2) is

$$\underline{R}_x^T(\hat{\underline{x}}(Ra); Ra)\underline{y}^* = \bar{\sigma}\underline{M}^T\underline{y}^* \quad , \tag{4.3}$$

where $\underline{y}^*$ is the adjoint eigenvector and $\bar{\sigma}$ is the complex conjugate of σ .
At Ra = Ra_c , σ is zero and the eigenvectors are the null vectors in eq. (3.22) with $\underline{u} = \underline{z}$ and $\underline{y}^* = \underline{y}$.

4.1 Exchange of Stability at a Limit Point

Consider a family of flows parameterized by the amplitude ϵ as $(\underline{x}(\epsilon), Ra(\epsilon))$ near a limit point at Ra = Ra_c and corresponding to $\epsilon = 0$. Expanding the eigenvalue and eigenvector in eq. (4.2) for small ϵ, taking the inner-product with respect to $\underline{y}$, and evaluating at $\epsilon = 0$ yields

$$\left[\frac{d\sigma}{d\epsilon}\right]_{\epsilon=0} = \frac{\underline{y}^T\underline{R}_{xx}\underline{x}_{(1)}\underline{z} + (\underline{y}^T\underline{R}x_{Ra}\underline{z})Ra_{(1)}}{\underline{y}^T\underline{M}\underline{z}} \quad , \tag{4.4}$$

where the derivatives of $\underline{R}$ are evaluated at $\underline{x}(0)$ and Ra(0). At a limit point, $Ra_{(1)}$ is zero, $\underline{x}_{(1)} = A\underline{z}$ and (4.4) reduces to

$$\left[\frac{d\sigma}{d\epsilon}\right]_{\epsilon=0} = \frac{A(\underline{y}^T\underline{R}_{xx}\underline{z}\underline{z})}{(\underline{y}^T\underline{M}\underline{z})} \quad . \tag{4.5}$$

The constant A is most efficiently eliminated from (4.5) by introducing eq. (3.26) as the definition of ϵ which gives $A \equiv 1$. Equation (4.5) is simplified further by introducing the solvability condition for the second-order problem (3.19) evaluated at the limit point;

$$Ra_{(2)} = \frac{\underline{y}^T\underline{R}_{xx}\underline{z}\underline{z}}{\underline{R}_{Ra}^T\underline{y}} \quad . \tag{4.6}$$

Substituting (4.6) into (4.5) gives the criterion for evaluating stability
at a limit point as

$$\left[\frac{d\sigma}{d\epsilon}\right]_{\epsilon=0} = -Ra_{(2)} \frac{\underline{y}^T \underline{R}_{Ra}}{\underline{y}^T \underline{Mz}} \qquad . \tag{4.7}$$

We evaluate the sign of $Ra_{(2)}$ from flows and their corresponding value
of ϵ on both sides of the limit point and calculate the ratio $\underline{y}^T \underline{R}_{Ra}/\underline{y}^T \underline{Mz}$
using the adjoint null vector determined from eq. (3.22). The criterion
(4.7) has been derived by Szeto (1978) and by Ungar and Brown (1983) using
an alternative approach.

4.2 Exchange of Stability at a Bifurcation Point

Equation (4.4) gives the direction for the crossing of the eigenvalue
through zero at either a bifurcation or limit point. Along the primary
family, we assume that $Ra_{(1)}$ is not zero and (4.4) is rewritten in terms
of the coefficients in the bifurcation equation (3.28)

$$\left[\frac{d\sigma}{d\epsilon}\right]_{\epsilon=0} = \frac{AC_1 + C_2 Ra_{(1)}}{(\underline{y}^T \underline{Mz})} \qquad , \tag{4.8}$$

as first presented by Szeto (1978). The criterion (4.8) can be evaluated
along either the primary or the bifurcating family using the pairs $(A, Ra_{(1)})$
determined as roots of eqs. (3.27, 3.28) and is sufficient for determining
exchanges of stability unless $Ra_{(1)}$ is zero, that is, unless the bifurcation
is super- or sub-critical. Then $d\sigma/d\epsilon = 0$ along the bifurcating family and
stability is determined by the second-derivative $(d^2\sigma/d\epsilon^2)_{\epsilon=0}$. Szeto (1978)
has developed a formula for this coefficient that involves the third derivative

$\underline{R}_{xxx}$ evaluate at the bifurcation point, a difficult quantity to calculate. Instead of using this result, we develop a more easily evaluated criterion based on the approach of Iooss and Joseph (1980) of linking the shapes of the bifurcating families to the exchange of stability along the primary family.

2. Super- and Sub-Critical Bifurcation Points

The equation set (3.10) is recast into local form expressed about the known, primary solution family $(\hat{\underline{x}}(\epsilon), \hat{Ra}(\epsilon))$ by defining the new vector $\underline{w}(\epsilon) \equiv \underline{x}(\epsilon) - \hat{\underline{x}}(\epsilon)$ and the equation set

$$\frac{d\underline{w}}{dt} = \underline{f}(\underline{w}; Ra(\epsilon)) \equiv \underline{R}(\underline{w} + \hat{\underline{x}}(\epsilon); Ra(\epsilon)) - \underline{R}(\hat{\underline{x}}(\epsilon); \hat{Ra}(\epsilon)) \quad . \qquad (4.9)$$

Equations (4.9) have the steady solution $\underline{w}(\epsilon) = \underline{0}$ and the vector $\underline{f}(\underline{w}; Ra(\epsilon))$ also satisfies the conditions

$$\frac{\partial^k \underline{f}}{\partial Ra^k} (\underline{0}; Ra(\epsilon)) = \underline{0} \qquad , \qquad (4.10)$$

for all values of k.

The form of the bifurcating family is analyzed by constructing an expansion in ϵ of $\underline{w}(\epsilon)$ and $Ra(\epsilon)$ similar to eq. (3.17). In this local form, the first-order corrections are governed by

$$\underline{f}_{\underline{w}}(\underline{w}(\epsilon); Ra(\epsilon))\underline{w}_\epsilon(\epsilon) + Ra_\epsilon(\epsilon)\underline{f}_{Ra}(\underline{w}(\epsilon); Ra(\epsilon)) = \underline{0} \quad , \qquad (4.11)$$

with the subscript ϵ standing for partial differentiation. When quantities in eq. (4.11) are evaluated at the bifurcation point ($\epsilon = 0$) this equation is analogous to eq. (3.18) . However, the condition eq. (4.10) with $k = 1$ then reduces (4.11) to a homogeneous equation for $\underline{w}_\epsilon(0) \equiv \underline{w}_{(1)}(0)$ which has

a component only in the null space of the Jacobian matrix $\underline{f}$ (0; Ra(0)) $\equiv$ $\underline{f}_x(\hat{\underline{x}}(0); \hat{Ra}(0))$. Hence, the tangent vector in local form is, in some sense, strictly normal to the primary flow, that is

$$\underline{w}_\epsilon(\epsilon) = \underline{z} + \mathcal{O}(\epsilon) \qquad . \tag{4.12}$$

The stability of the flows along the bifurcating family $(\underline{w}(\epsilon), Ra(\epsilon))$ is resolved in terms of an eigenvalue problem form by perturbing these steady solutions as $\underline{w}(t;\epsilon) = \underline{w}(\epsilon) + \underline{\zeta}e^{\gamma t}$, where the magnitude of $\underline{\zeta}$ is small. This eigenvalue problem is

$$\underline{f}_w(\underline{w}(\epsilon); Ra(\epsilon))\underline{\zeta} = \gamma(\epsilon)\underline{\underline{M}}\underline{\zeta} \qquad , \tag{4.13}$$

and its adjoint is

$$\underline{f}_w^T(\underline{w}(\epsilon); Ra(\epsilon))\underline{\zeta}^* = \overline{\gamma}(\epsilon)\underline{\underline{M}}^T\underline{\zeta}^* \qquad , \tag{4.14}$$

where $\underline{\zeta}^*$ is the adjoint eigenvector.

An equation for the eigenvalue $\gamma(\epsilon)$ valid for any flow in the bifurcating family is derived by forming the inner product between $\underline{\zeta}^*$ and the first-order problem (4.11) and by using the relationship

$$\underline{\zeta}^{*T}\underline{f}_w\underline{w}_\epsilon = \underline{f}_w^T\underline{\zeta}^*\underline{w}_\epsilon = \overline{\gamma}(\epsilon)\underline{\underline{M}}^T\underline{\zeta}^*\underline{w}_\epsilon \qquad . \tag{4.15}$$

Then $\gamma(\epsilon)$ is given by

$$\gamma(\epsilon) = -Ra_\epsilon(\epsilon) \frac{\underline{\zeta}^{*T}\underline{f}_{Ra}(\underline{w}(\epsilon); Ra(\epsilon))}{\underline{\underline{M}}^T\underline{\zeta}^*\underline{w}_\epsilon} \qquad . \tag{4.16}$$

A useful criterion for assessing stability at sub- or super-critical bifurcation points is derived by expanding the right hand side of (4.16) for small ϵ using the result (4.12) and the relationships $Ra_\epsilon(\epsilon) = Ra_{(1)} + Ra_{(2)}\epsilon + O(\epsilon^2)$,

$\underline{z}^* = \underline{y} + O(\epsilon)$, and $\underline{f}_{Ra}(\underline{w}(\epsilon); Ra(\epsilon)) = \underline{f}_{wRa}(\underline{0}; Ra(0)\underline{z} \epsilon + O(\epsilon^2) = \underline{R}_{xRa}(\hat{\underline{x}}(0); \hat{Ra}(0))\underline{z}\epsilon + O(\epsilon^2)$. Then eq. (4.16) reduces to

$$\gamma(\epsilon) = -Ra_{(2)} \frac{\underline{y}^T \underline{R}_{xRa}(\hat{\underline{x}}(0); \hat{Ra}(0))\underline{z}\epsilon^2}{\underline{y}^T \underline{M}\underline{z}} + O(\epsilon^3) , \qquad (4.17)$$

which is re-written in terms of the slope of the eigenvalue σ along the primary flow family as

$$\gamma(\epsilon) = \frac{-Ra_{(2)}(d\sigma/d\epsilon)_{\epsilon=0}}{(dRa/d\epsilon)_{\epsilon=0}} \epsilon^2 + O(\epsilon^3) , \qquad (4.18)$$

where $(dRa/d\epsilon)_{\epsilon=0}$ is the slope of the primary family at the bifurcation point and $(d\sigma/d\epsilon)_{\epsilon=0}$ is the slope of the critical eigenvalue. The result (4.18) is equivalent to the Factorization Theorem derived by Iooss and Joseph (1980) and gives the stability of the bifurcating family in terms of its evolution near the bifurcation point and the exchange of stability along the primary flow family.

5. CALCULATION OF THE ONSET OF CONVECTION

The critical values of Rayleigh number where steady flows branch from the static state have been calculated by monitoring the determinant of the Jacobian matrix evaluated about this state. This determinant is plotted on Figure 2 for a cylinder with $\Lambda=0.5$ and insulated sidewall, as calculated with a mesh composed of four elements in each of the axial and radial directions. This mesh leads to a set of 224 nonlinear equations. The calculations were performed with $Pr=1.0$, however the critical values of Rayleigh number determined are independent of Prandtl number. Although the determinant of $\underline{J}$ is extremely small in an absolute sense, its roots in terms of Ra are clearly seen in Figure 2 and can be systematically refined by numerical bisection. In most cases, we located the roots of $\det(\underline{J})$ to within ± 5 in Rayleigh number.

The lowest three critical values ($Ra_c^{(1)}$, $Ra_c^{(2)}$, $Ra_c^{(3)}$) calculated here are compared in Table I to results reported by Charlson and Sani (1970) for cylinders with insulated sidewalls and aspect ratios between 0.5 and 2.70. The meshes used in our calculations were varied so that the size of the elements remained essentially constant over this range of aspect ratio. The finite element results agree well with those of Charlson and Sani, even for these relatively coarse discretizations. The structure of the flow field also is represented on Table I by the number of toroidal roll cells in the axial and radial directions; for example, 2R denotes a flow with two toroidal cells nested radially in the cylinder. For small Λ, our ordering of the second and third critical Rayleigh numbers does not agree with Charlson and Sani, who didn't report flows with more than one cell in the axial direction.

Increasing the number of elements in the mesh leads to more accurate results for the values of Ra_c and the corresponding eigenfunctions. This point is demonstrated by Table II where the lowest two critical values $(Ra_c^{(1)}, Ra_c^{(2)})$ are listed as a function of mesh for a cylinder with an insulated sidewall and $\Lambda=1.0$. Both values varied by less than 0.6% for meshes of between 4x4 and 8x8 elements. The values of Ra at the first several bifurcation points are plotted on Figure 3 as a function of aspect ratio. The structure of the flow fields that evolve from these critical values are indicated by contours of the streamfunction shown for each curve and plotted more exactly on Figure 4. The flow field originating at the lowest value of Ra_c evolves continuously with Λ from a single cell, to a two, and then to a three cell flow; see the plots for the lowest values of Ra_c on Figure 4.

For the calculations presented here with no-slip boundary conditions on all surfaces, there were no crossings of the curves of the lowest two values of Ra_c; the only sharp interchange of the ordering of two bifurcating families was found between the second and third critical values near $\Lambda \equiv \Lambda_c = 0.715$. The second critical point $Ra_c^{(2)} = Ra_c^{(3)}$ for this aspect ratio was a second-order critical point with two linearly independent eigenfunctions and hence had a Reisz Index of one (see Iooss and Joseph 1981). The role of this point in the nonlinear evolution of the flow structure is brought out in §7.2.

6. FINITE AMPLITUDE FLOW FIELDS: $\Lambda = 1.0$

The finite element approximations and computer-aided methods for tracking multiple solutions to algebraic equations have been used to calculate flow fields in the families emanating from the lowest four critical values of Rayleigh number for a cylinder with aspect ratio $\Lambda = 1.0$ and an insulated sidewall. Here and throughout the remainder of this report the fluid is taken to have a Prandtl number of one. Flow fields in each family close to Ra_c were found by using the first approximation eq. (3.23) with the corresponding eigenvector. Experience from weakly nonlinear analysis of Rayleigh-Bénard problems (Schluter et al.; Rosenblat 1982) and other finite amplitude calculations for the cylindrical geometry (Liang et al. 1969; Charlson and Sani 1975) suggested that the bifurcating families evolve supercritically in Rayleigh number (towards increasing Ra). We searched for, and always found, the new flow families at $(Ra-Ra_c)$ greater than zero near Ra_c. The direction of the flows (either up or down along the centerline of the cylinder) in a particular family was arbitrary and pointed to two distinct families evolving from each bifurcation point. Both were computed by changing the otherwise arbitrary sign of the constant A in eq. (3.23).

The flow families computed with a 4x4 mesh are represented on Figure 5 as a plot of the average Nusselt number between the top and bottom surfaces of the cylinder as a function of Ra. Since the sidewall was insulated, the heat fluxes through the top and bottom should have been the same and these two Nusselt numbers should have been equal. As discussed below, the discretization error in the finite element approximation prevented this condition

from being satisfied. Flows composed of a single roll cell moving either up (1U) or down (1D) along the centerline developed for $Ra > Ra_c$; sample streamlines and isotherms from the 1D family are shown in Figure 6. At large values of $Ra - Ra_c$ these flows developed a small secondary vortex in the upper corner of the cylinder which grew with increasing Ra. This secondary flow was found only for values of Rayleigh beyond those calculated by Charlson and Sani (1975).

The flow families that bifurcated from the second critical value $Ra_c^{(2)}$ had two cells nested radially. Again there were two families of flows that differed only by the direction of the axial motion along the centerline; we called these the 2RU and 2RD families, where the 2R designation represented the radial structure of the flow. Sample streamfunctions and isotherms for flows in the 2RD family are displayed as Figure 7. As the Rayleigh number increased the purely radial orientation of the cells was lost and the flow evolved toward the same cellular configuration shown in Figure 6 for the 1D family.

Neither the (1D, 1U) or the (2RD, 2RU) families existed for Ra beyond a critical value $Ra_\ell \approx 2.3 \times 10^4$, where the two families connected to form a continuous solution curve; the value $Ra = Ra_\ell$ is a limit point. The arguments for evaluating linear stability put forth in §4 show that the static solution lost stability at $Ra = Ra_c^{(1)}$, as found by Charlson and Sani (1970), and that the 1U and 1D flow families were stable. These flows lost stability at the limit point. The flows in the 2RU and 2RD families were all unstable. The stability of the flows in each familiy is shown on Figure 5 by solid (stable) and dashed (unstable) curves.

The flow families that bifurcated from the third $Ra_c^{(3)}$ and four $Ra_c^{(4)}$

critical values are also shown on Figure 5. Flows in the families evolving from $Ra_c^{(3)}$ had three radially nest cells (3RU and 3RD) and passed quickly through a limit point in Rayleigh number. The flows associated with $Ra_c^{(4)}$ had two roll cells stacked axially on top of each other. We called these families 2ASD and 2ASU, where the 2A designated the two axial cells, S stood for the plane of reflective symmetry through z=1/2 which divided the cells, and the D and U described whether the flow in the top cell was down or up along the centerline. Interestingly, these families were connected by a secondary bifurcation point on the 2ASU family. Two other points of secondary bifurcation were also located on the 2ASD family, but because of the 2ASD flows were already unstable, the flow families evolving from these critical points were not calculated.

The nonlinear connection of two families that appeared to be distinct in linear analysis was an important result of the results for Λ=1.0 and was found at all values of aspect ratio. We pause here to show that this phenomena was not an artifact of the coarse finite element approximation, but was indeed present for calculations with finer meshes. This point is made by examining Figure 8 where the results of tracking the 1D and 2RD flow families are shown for four different finite element discretizations; clearly, all three sets of calculations were in qualitative agreement and the 6x6 and 8x8 meshes gave very similar results, indicating convergence of the calculation with mesh refinement.

We also attempted to compare the Nusselt numbers calculated for flows in the 1D family near the critcal value $Ra_c^{(1)}$ with those reported in Charlson and Sani (1975), but found the Nusselt numbers reported there to be much smaller than either the values we calculated or the values reported by Jones et al. (1976) for cylinders with large aspect ratio and shear-free sidewalls. Another

comparison between our calculations and those of Charlson and Sani was made
by calculating the flows that evolve from the lowest critical Rayleigh number
for a cylinder with Λ=1.0 and a perfectly conducting sidewall. The Nusselt
numbers evaluated at the top and bottom surfaces are plotted for this case
in Figure 9 for two finite element grids along with the numbers reported by
Charlson and Sani (1975). The sets of calculations are in good agreement,
with the finite element results converging to those of Charlson and Sani for
the finest mesh used. The 1D family reached a limiting value of Ra for a
cylinder with conducting sidewalls, just as it did for the perfectly insulated
case; this case is discussed in more detail in another publication (Brown et al.
1983).

7. EVOLUTION OF NONLINEAR FLOW STRUCTURE WITH ASPECT RATIO

The double point found between the second and third critical Rayleigh num-
bers at $\Lambda \equiv \Lambda_c \approx 0.715$ (see Figure 3) hints that the nonlinear structure of the
steady flows may undergo qualitative changes with varying aspect ratio. In
this Section, we report results for aspect ratios between 0.5 and 2.00 for a
fluid with $Pr \approx 1.0$ in cylinders with insulated sidewalls. The enormous number
of calculations (almost 1500) needed to carry out this study has necessitated
using the coarse finite element meshes listed in Table I for each value of
Λ. Although calculations with these meshes may have errors in the overall
heat balance of as much as ten percent for a few of the more vigorous flows,
the checks of accuracy for $\Lambda=1.0$ discussed in §6 and mesh refinement of several
of the calculations reported in this section give confidence that the quali-
tative behavior of the flow fields are correct.

7.1 The case $\Lambda=0.5$

The flow families that evolved from the lowest two values of Ra_c are
represented on Figure 10 for $\Lambda=0.5$ and $Pr = 1.0$. Just as for the cylinder
with $\Lambda=1.0$, flows composed of a single roll cell (1U and 1D families) developed
for $Ra > Ra_c^{(1)}$ up to a limiting value of Rayleigh numbers $Ra \equiv Ra^{\ell}$. Repre-
sentative streamlines for flows in the 1D family are shown in Figure 11 and
again developed a small secondary cell in the upper corner of the cylinder
which intensifies with increasing Ra up to Ra^{ℓ}. The evolution of the 1D and
1U families past the limit point differed from the structure for the same flow
families with $\Lambda=1.0$ discussed in §6.

For $\Lambda=0.5$, the flow fields that bifurcated from $Ra=Ra_c^{(2)}$ had two cells
stacked axially (2ASU and 2ASD) and also evolved toward higher values of Ra;

flows in the 2AUS family are shown in Figure 12. The plane of symmetry between the two cells was broken at secondary bifurcation points to new flow families, as indicated on Figure 11. The new flows branching from the 2ASU family are denoted as 2AUU and 2AUD, where the first U in both labels indicates that the top cell was circulating upward along the center-line and the suffices U and D indicate whether the top (U) or bottom (D) cell was the strongest. Members of the 2AUD family are displayed in Figure 13 to show that velocity fields away from the secondary bifurcation point had so large a bottom cell that the top one was pushed into the upper right hand corner of the cylinder and that the flows closely resembled those in the 1D family. As implied by this remark, the 1D and 2AUS families were connected along the solution curve that lead to the limit point $Ra=Ra^{\ell}$.

The stability of the flows in these two families was determined entirely on the basis of the results for the stability of the flows emanating from the static state, the numerical calculation of Ra^{ℓ} as a simple limit point and the connectivity of the flow families. As shown on Figure 11, only the 1U and 1D flow families are stable in the sense described in §4.

7.2 Flows near the double point: $\Lambda \equiv \Lambda_c \approx 0.715$

The double point at $\Lambda = \Lambda_c \approx 0.715$ between the 2A and 2R families marked the first change in the flow structure from that shown for $\Lambda = 0.5$. The flows computed for aspect ratios of 0.71 and 0.72, which bracket this double point, are represented in Figures 14 and 15. For $\Lambda = 0.71$, the first two families have 1U and 2A flow patterns and are connected at a secondary bifurcation point along the 2ASU branch, as was the case for $\Lambda = 0.50$. The only change in the single-cell flows between $\Lambda = 0.5$ and 0.71 was the development of a pair of limit points in this family and the creation of a new segment of stable flows;

this behavior is depicted in Figure 14. At $\Lambda=0.71$ a secondary bifurcation point was found along the 2ASD family (two symmetric axial cells with the top cell flowing down at the centerline) and the flows evolving from this point evolved continuously with increasing Rayleigh number into 2RU and 2RD flows.

Changing the aspect ratio so that $\Lambda>\Lambda_c$ did not alter the connectivity of the 1U, 1R and 2ASU families, but switched the order of appearance of the 2R and 2A families and moved the secondary bifurcation point from the 2ASD to the 2ASU branch. The change of the secondary bifurcation point as the apsect ratio passes through the double point $\Lambda = \Lambda_c$ is anticipated from the asymptotic theories of Bauer et al. (1975) and Keener (1976) for bifurcation near such a second-order singularity. The connectivity between the 2R and 2A flow families was not forecasted, although a similar structure occurred in the reaction-diffusion problem studied by Keener (1976). Figure 16 shows the evolution of the 2A and 2R families that we conjecture as Λ is varied through Λ_c. Because of the connectivity between the two families and the switching of the secondary bifurcation point from the 2ASD to the 2ASU families only the 2AU and 2AD flows are thought to exist at Λ exactly equal to Λ_c.

7.3 Change in Flow Family Connectivity by Multiple Limit Point Bifurcation

Varying the aspect ratio between 0.72 and 1.00 resulted in the loss of the secondary bifurcation point pictured in Figures 14-16 and the connectivity of the first two flow families shown in Figure 5. Evidence for the cause of this transition is displayed in the structure of the 2R and 2A flow families for $\Lambda=0.75$ and 0.85 shown in Figure 17. At the lower aspect ratio the connectivity between the 2R and 2A was essentially the same as discussed for

Λ=0.72. However, at Λ=0.85 the 2R and 2A flow families were no longer connected and the two secondary bifurcation points along the 2ASU family were found to join a single family of flows. The 2R flows evolved continuously into the single-celled flows.

The differences in structure between Λ=0.75 and 0.85 suggests that the flows emanating from the secondary bifurcation points interacted for $\Lambda = \Lambda^*$, $0.75 \leq \Lambda^* \leq 0.85$, in a way that replaced the coupling between the single-cell and 2A flows and resulted in the formation of continuous paths between the 1U, 1D, 2RU and 2RD branches. Multiple-limit-point bifurcation, as discussed by Decker and Keller (1980), is a possible mechanism for this transition. The transitions through a multiple-limit-point are sketched in Figure 18; here, the limit points in the 2R and 2AU families would coalesce at $\Lambda = \Lambda^*$ and exchange connectivity, thereby leading to the structure shown for $\Lambda > \Lambda_c$.

7.4 The case Λ=2.0

Increasing the aspect ratio beyond $\Lambda = \Lambda^*$ did not change the connectivity of the flow families bifurcating from $Ra_{(1)}$ and $Ra_{(2)}$ shown for Λ=0 (see Figure 15). At large aspect ratio both families were composed of f s with two radially nested cells, which only differed in relative intensi , streamlines for sample flows in both families are shown in Figure 20. The flow patterns in two families that evolve from $Ra_c^{(1)}$ and $Ra_c^{(2)}$ both have two radial cells but differ according to whether the inner or outermost cell is the most intense. Near the limit point, $Ra=R_\ell \approx 3.2\times10^4$, the two families converge with the outer cell driving the weaker inner cell to the centerline of the cylinder.

A second set of flows bifurcating from $Ra_c^{(3)}$ and $Ra_c^{(4)}$ were also calculated and evolved as a continuous loop with three radial cells (3R) in the

first family and four cells (4R) in the second. The coarse 10x4 mesh made it difficult to accurately resolve these velocity and temperature fields at Rayleigh numbers much above the critical values. The qualitative structure of the 3R and 4R flow families is most probably accurate; however, calculations with more refined meshes are needed to accurately calculate the value for Ra at the limit point.

Starting from an initial approximation and continuation vector calculated for a flow belonging to the family that bifurcated from $Ra_c^{(1)}$, the Newton iterations converged to a flow in a new family. We tracked the family from this starting point and found it to evolve as a closed loop or isola which was not connected by bifurcation points to any other flows. Flows throughout the isola were composed of a dominant cell with motion up along the centerline, with a small counter-clockwise vortex in the lower corner of the cylinder. Sample streamlines along both the upper (with respect to Nusselt number) and lower branches of the isola are shown in Figure 21. The limit points which connected these two families mark changes in the relative stability of the two families, but the absolute stability of these flows could not be determined without either an understanding of the mechanism for creation of the isola from flow families originally connected to the static family or numerical calculation of the eigenvalues in eq. (4.2).

We attempted to trace the evolution of the isola by numerically continuing solutions in the loop for $\Lambda=2.0$ at given Rayleigh numbers ($Ra=1.0 \times 10^4$ and 4×10^4) to lower values of aspect ratio. An isola was successfully located for $\Lambda=1.8$. Attempts to locate the isola at $\Lambda=1.4$ resulted only in calculation of flows in the 2R family. At this aspect ratio families of single-cell and 2R flows bifurcating from $Ra_c^{(1)}$ and $Ra_c^{(2)}$ were connected at a limit point $Ra \equiv Ra_\ell \approx 5.8 \times 10^4$, which this value for Ra_ℓ was significantly higher than calculated for either $\Lambda=1.0$ or 2.0 .

The flow fields calculated for $Ra = 1.0 \times 10^4$ and 4.0×10^4 with $1.4 \leq \Lambda \leq 1.8$ are shown in Figure 22 and seemed to indicate that a continuous path in the solution space was traced. This result and the decrease in Ra_λ between aspect ratios of 1.4 and 2.0 gave credence to the idea that the isola was created by the creation of singular points along the 2R family. The only candidate seemed to be the pinching of the loop to a point of self-intersection and finally to separation. This mechanism for isola generation has been documented in models from reaction engineering (Uppal et al. 1976) and leads to the interesting conjecture that one branch of the isola may be composed of stable flows. We have not tried to analyze the creation of the isola beyond the results reported here. Again, finer finite element meshes may be necessary to resolve this detail.

8. DISCUSSION

The most significant finding of this study was the connectivity pre-
dicted between families of axisymmetric flows which originated at adjacent
critical Rayleigh numbers. A continuous path of axisymmetric flows was
found for all aspect ratios tested between 0.5 and 2.00 . The details
of the path, i.e. whether it involved only a limit point or included sec-
ondary bifurcation, did depend on aspect ratio. Imperfections in the ther-
mal boundary conditions, which introduce radial temperature gradients, rup-
ture both the primary and secondary bifurcation points calculated here, as
described by the analysis of Hall and Walton (1976). The connectivity be-
tween the first and second axisymmetric families then is by a limit point
along a continuous path for $0.5 \leq \Lambda \leq 2.70$.

Connectivity between bifurcating families has not been detected in the
previous asymptotic analyses of convection in either rectangular slits (Hall
and Walton 1979) or cylinders with shear-free boundaries (Rosenblat 1982).
Both analyses focused on values of aspect ratio for semi-simple double points.
The first two double points between axisymmetric flows are represented on
Figure 1 for a cylinder with shear-free boundaries. Neither of these second-
order critical points exists for a cylinder with no-slip boundaries, as shown
on Figure 3. We believe the imperfection in the spectrum of the linearized
problem caused by varying the boundary conditions on the tangential velocity
plays a major role in establishing the connectivity between solution families
observed here, but not seen in calculations for cylinders with shear-free
sidewalls (Jones et al. 1976; Brown 1983). A systematic asymptotic study of
convection in cylinders with slightly sticky boundaries is underway.

The calculations presented where are only the first step toward a compre-
hensive understanding of convective transitions in a cylinder heated from below.

Three-dimensional and time-periodic flows are almost unexplored theoretically. Nonaxisymmetric convection modes are known (Charlson and Sani 1971) to be most dangerous at large and small values of Λ of a rigid cylinder. Even when an axisymmetric mode is the first to bifurcate, as is the case for $Pr=1.0$ and $\Lambda=1.0$, three-dimensional convection may dominate after a secondary bifurcation, as demonstrated by a few calculations in Charlson and Sani (1975) for a cylinder with conducting sidewalls. Three-dimensional convection patterns and time periodic flows have been reported by Olson and Rosenberger (1979) for gases in a cylinder with $\Lambda=1/6$ heated from below for Rayleigh numbers 5.86 times $Ra_c^{(1)}$. The numerical value of Ra for the onset of oscillations is no doubt a function of both aspect ratio and Prandtl number.

The strategy presented here for computing steady flows and analyzing non-linear structure and stability generalizes to the study of three-dimensional flows by the finite element method and to other numerical approximations for computing two-dimensional convection which incorporate Newton's method for solution of the full set of residual equations (van Steeg and Wesseling 1978; McDonough and Catton 1982). Only the availability of large, fast super-computers limits this approach, as it did for the pioneering calculations of Charlson and Sani (1975). Nonaxisymmetric calculations are now feasible in geometries where the boundary conditions allow spectral representation of the azimuthal dependence of the field variables. New numerical approximations that are a hybrid of spectral and finite element approximations are being developed for calculating steady three-dimensional convection in a cylinder.

Just as in asymptotic expansions based on eigen-modes, care must be taken to access the range of validity of the numerical appoximation at large values of $|Ra-Ra_c|$ or when the flow pattern involves multiple cells. Spurious steady

solutions to discretized equations have been reported in several studies (Schrieber and Keller 1983; Chang and Brown 1983; Yeh et al. 1983) when the numerical approximation, either finite difference or finite element, cannot resolve boundary layers and separation in a flow field. Similar numerical artifacts can result at low values of $|Ra-Ra_c|$ when the finite element approximation is insufficient to resolve multiple flow cells; this limitation has restricted our calculations to Λ less than 3. Spectral decompositions are better suited to calculations at large Λ.

REFERENCES

Bauer, L., Keller, H.B. and Reiss, E.L. 1975 Multiple eigenvalues lead to secondary bifurcation. SIAM Review 17, 101-122.

Bénard, H. 1901 Les tourbillens cellulaires dans une nappe liquide transportant de la chaleur par convection en régime permanent. Ann. Chim. Phys. 23, 62-144.

Brown, R.A. 1983 The structure of axisymmetric steady convection in a vertical cylinder. In Nonlinear Dynamics (ed. V. Hlavacek). New York: Gordon and Breach.

Brown, R.A. and Scriven, L.E. 1980a The shapes and stability of captive rotating drops. Phil. Trans. R. Soc. Lond. A297, 51-79.

Brown, R.A. and Scriven, L.E. 1980b The shape and stability of rotating liquid drops. Proc. R. Soc. Lond. A371, 331-357.

Brown, R.A., Scriven, L.E., and Silliman, W.J. 1980 Computer-aided analysis of nonlinear problems in transport phenomena. In New Methods in Nonlinear Dynamics (ed. P. Holmes). Philadelphia: SIAM.

Brown, S.N. and Stewartson, K. 1978 On finite amplitude Bénard convection in a cylindrical container. Proc. R. Soc. Lond. A360, 455-469.

Brown, S.N. and Stewartson, K. 1979 On finite-amplitude Bénard convection in a cylindrical container. Part II. SIAM J. Appl. Math. 36, 573-586.

Chandrasekhar, S. 1961 Hydrodynamic and Hydromagnetic Stability. Oxford: Oxford Press.

Chang, C.J. and Brown, R.A. 1983 Radial segregation induced by natural convection and melt/solid interface shape in vertical Bridgman growth. J. Crystal Growth, in press.

Charlson, G.S. and Sani, R.L. 1970 Thermoconvective instability in a bounded cylindrical fluid layer. Int. J. Heat Mass Transfer 13, 1479-1496.

Charlson, G.C. and Sani, R.L. 1971 On thermoconvective instability in a bounded cylindrical fluid layer. Int. J. Heat Mass Transfer. 14, 2157-2160.

Charlson, G.S. and Sani, R.L. 1975 Finite amplitude axisymmetric thermoconvective flows in a bounded cylindrical layer of fluid. J. Fluid Mech. 21, 209-229.

Daniels, P.G. 1977 The effect of distant sidewalls on the transition to finite amplitude Bénard convection. Proc. R. Soc. Lond. A. 358, 173-197.

Davis, S.H. 1967 Convection in a box: linear theory. J. Fluid Mech. 30, 465-478.

Decker, D.W. and Keller, H.B. 1980 Multiple limit point bifurcation. J. Math. Anal. Appl. 75, 417-430.

Hall, P. and Walton, I.C. 1977 The smooth transition to a convective regime in a two-dimensional box. Proc. R. Soc. London A358, 199-221.

Hall, P. and Walton, I.C. 1979 Bénard convection in a finite box: secondary and imperfect bifurcations. J. Fluid Mech. 90, 377-395.

Hood, P. 1976 Frontal solution program for unsymmetric matrices. Int. J. Num. Meth. in Engng. 10, 379-399.

Huyakorn, P., Taylor, C., Lee, R. and Gresho, P. 1978 A comparison of various mixed-interpolation finite elements in the velocity-pressure formulation of the Navier-Stokes equations, Computers and Fluids 6, 25-35.

Iooss, G. and Joseph, D.D. 1980 Elementary Stability and Bifurcation Theory. New York: Springer-Verlag.

Jones, C.A., Moore, D.R., and Weiss, N.D. 1976 Axisymmetric Convection in a Cylinder. J. Fluid Mech. 73 353-388.

Joseph, D.D. 1971 Stability of convection in containers of arbitrary shape. J. Fluid Mech. 47, 257-282.

Keener, J.P. 1976 Secondary bifurcations in non-linear diffusion reaction equations. Stud. Appl. Math. 55, 187-211 (1976).

Keller, H.B., 1980 Two new bifurcation phenomena. In Applications of Nonlinear Analysis in the Physical Sciences (ed. H. Amann, H. Bazley, K. Kirchgässner). New York: Pitman.

Keller, H.B., 1977 Numerical solution of bifurcation and nonlinear eigenvalue problems. In Applications of Bifurcation Theory (ed. P.H. Rabinowitz). New York: Academic Press.

Kelly, R.E. and Pal, D. 1976 Thermal convection between nonuniformly heat horizontal surfaces. Proc. 1976 Heat Transfer and Fluid Mechanics Inst. Stanford: Stanford University Press.

Kubicek, M. 1976 Dependence of solution of nonlinear equations on a parameter. ACM Trans. Math. Software 2, 98-107.

Liang, S.F., Vidal, A., and Acrivos, A. 1969 Buoyancy-driven convection in cylindrical geometries. J. Fluid Mech. 86, 239-256.

McDonough, J.M. and Catton, I. 1982 A mixed finite difference-Galerkin procedure for two-dimensional convection in a square box. Int. J. Heat Mass Transfer 25, 1137-1146.

Olson, J.M. and Rosenberger, F. 1979 Convective instabilities in a closed vertical cylinder heated from below. J. Fluid Mech. 92 609-629.

Rayleigh, Lord 1916 On convection currents in a horizontal layer of fluid when the higher temperature is on the under side. Phil. Mag. 32, 529-546.

Rheinboldt, W.C. 1978 Numerical methods for a class of finite dimensional bifurcation problems. SIAM Jl Numer. Anal. 15, 1-11.

Riks, E. 1972 The application of Newton's method to the problem of elastic stability. J. Appl. Mech. 39, 1060-1065.

Rosenblat, S. 1982 Thermal convection in a vertical circular cylinder. J. Fluid. Mech. 122, 395-410.

Schlüter, A., Lortz, D. and Busse, F. 1965 On the stability of steady finite amplitude convection. J. Fluid Mech. 23, 129-144.

Schreiber, R. and Keller, H.B. 1983 Spurious solutions in driven cavity calculations. J. Computat. Physics 49, 165-172.

Steeg, J.G. van and Wesseling, P. 1978 Solution of the Boussinesq equations by means of the finite element method. Computers and Fluids 6, 93-101.

Szeto, R.K.H. 1978 The flow between rotating coaxial disks. Ph.D. thesis, California Institute of Technology.

Tavantis, J., Reiss, L. and Matkowsky, J. 1978 On the smooth transition to convection. SIAM J. Appl. Math. 34, 322-337.

Taylor, C. and Ijam, A.Z. 1979. A finite element numerical solution of natural convection in enclosed cavities, Comp. Meths. Appl. Mech. Engng. 19, 429-446.

Thomasset, F. 1981 Implementation of Finite Element Methods for Navier-Stokes Equations. New York: Springer-Verlag.

Ungar, L.H. and Brown, R.A. 1982 The dependence of the shape and stability of captive rotating drops on multiple parameters. Phil. Trans. R. Soc. Lond. A306, 347-370.

Unger, L.H. and Brown, R.A. 1983 Cellular interface morphologies in directional solidification. Physical Review submitted.

Uppal, A., Ray, W.H. and Poore, A.B. 1976 The classification of the dynamic behavior of continuous stirred tank reactors - influence of reactor residence time. Chem. Engng. Sci. 31, 205-214.

Yeh, P.-W., Kim-E., M., Armstrong, R.C., and Brown, R.A. 1983 On the Deborah number limit for calculation of Maxwell fluid flowing through an axisymmetric contraction. J. Non-Newtonian Fluid Mech. to be submitted.

Zie⁻kiewiez, D.C., Gallagher, R.H. and Hood, P. 1976 Newtonian and non-Newtonian viscous incompressible flow. Temperature-induced flows. Finite element solutions. In The Mathematics of Finite Elements and Applications 2 (ed. J.R. Whiteman). London: Academic Press.

Zierep, J. 1963 Zur Theorie der Zellularkonektion V., Beit. Physik Atmos. 36, 70-76.

FIGURE CAPTIONS

Table I. Comparison of first three critical Rayleigh numbers calculated
by finite element analysis with values reported by Charlson and
Sani (1970) for cylinders with aspect ratios between 0.5 and
2.75 and insulated sidewalls. The mesh was adjusted to conform
with the aspect ratio of the cylinder.

Figure 1. Schematic of critical Rayleigh numbers $\{Ra_c^{(i)}\}$ as a function of
aspect ratio Λ for a cylinder with shear-free boundaries. Each
curve is associated with a particular flow structure and the
ordering of the modes is interchanged by crossing the critical
values Λ_c

Figure 2. Determinant of the Jacobian matrix evaluated about the static
state as a function of Rayleigh number for $\Lambda=0.5$ and for a 4x4
finite element mesh. The cylinder has insulated sidewalls.

Figure 3. Lowest several critical Rayleigh numbers for a cylinder with in-
sulated sidewalls as a function of aspect ratio Λ.

Figure 4. Contours of streamfunction for the eigenfunction corresponding
to the lowest three critical values of $\{Ra_c^{(i)}\}$ for aspect ratios
between 0.5 and 2.75.

Figure 5. Families of axisymmetric flow fields in a cylinder with insulated
sidewalls for $\Lambda=1.0$ and Pr=1.0 . Stable flows are shown by solid
(——) curves and unstable flows by dashed (---) ones.

Figure 6. Representative streamlines and isotherms for flows in the 1D
family that occur before the limiting value of Ra for $\Lambda=1.0$.

Figure 7. Representative streamlines and isotherms for flows in the 2RD
family for $\Lambda=1.0$. Each of these flows are unstable.

Figure 8.   Families of 1D and 2RD flows in a cylinder with insulated side-walls computed with four different finite element girds; Λ=1.0 and Pr=1.0 .

Figure 9.   Nusselt numbers at top and bottom surfaces of a cylinder with perfectly conducting sidewall; Λ=1.0 and Pr=1.0 . Finite element results for two meshes are shown along with the results of Charlson and Sani. (1975).

Figure 10. Families of axisymmetric flow fields in a cylinder with insulated sidewalls for Λ=0.5 and Pr=1.0 . Stable flows are denoted by solid (——) curves and unstable flows by dashed (---) ones.

Figure 11. Representative streamlines and isotherms for flows in the 1D family that occur before the limiting value Ra^{ℓ} .

Figure 12. Representative streamlines and isotherms for flows in the 2ASU family.

Figure 13. Streamlines and isotherms for members of the 2AUD family which show the evolution of the flow field with changing Ra into the 1D family; compare with Figure 11.

Figure 14. Families of axisymmetric flow fields in a cylinder with insulated sidewalls for Λ=0.71 and Pr=1.0 . Stable flows are denoted by solid (——) curves and unstable flows by dashed (---) ones.

Figure 15. Families of axisymmetric flow fields in a cylinder with insulated sidewalls for Λ=0.72 and Pr=1.0 .

Figure 16. Evolution of flow families between families with two axial and two radial cells as aspect ratio is varied through Λ_c.

Figure 17. Structure of 2ASD, 2ASU and 2R flow families for Λ=0.75 and 0.85 ; Pr = 1.0

ASPECT RATIO	FINITE ELEMENT MESH	$Ra_c^{(1)}$				$Ra_c^{(2)}$				$Ra_c^{(3)}$			
		FEM	Charlson & Sani	% Diff.	MODE	FEM	Charlson & Sani	% Diff.	MODE	FEM	Charlson & Sani	% Diff.	MODE
0.50	4x8	10892	10887	0.05	1	28481	—	—	2A	69134	68048	0.13	2R
1.00	4x4	2270	2262	0.35	1	6678	6632	0.70	2R	20610	19266	6.98	3R
1.60	6x4	1933	1922	0.57	1	2456	2449	0.29	2R	4721	4701	0.13	3R
1.70	6x4	1956	1946	0.51	2R	2312	2304	0.35	2R	4076	4067	0.22	3R
2.00	8x4	1871	1862	0.48	2R	2344	2329	0.64	2R	2951	2940	0.37	3R
2.25	8x4	1800	1792	0.45	2R	2322	2315	0.30	3R	2744	2727	0.62	1R
2.70	10x4	1804	1793	0.61	2R	1977	1969	0.41	3R	2631	2629	0.08	4R

Table I. Comparison of lowest three critical Rayleigh numbers calculated by finite element analysis with values reported by Charlson and Sani (1970) for cylinders with aspect ratios between 0.5 and 2.75 and insulated sidewalls. The mesh has been adjusted to conform with the aspect ratio of the cylinder.
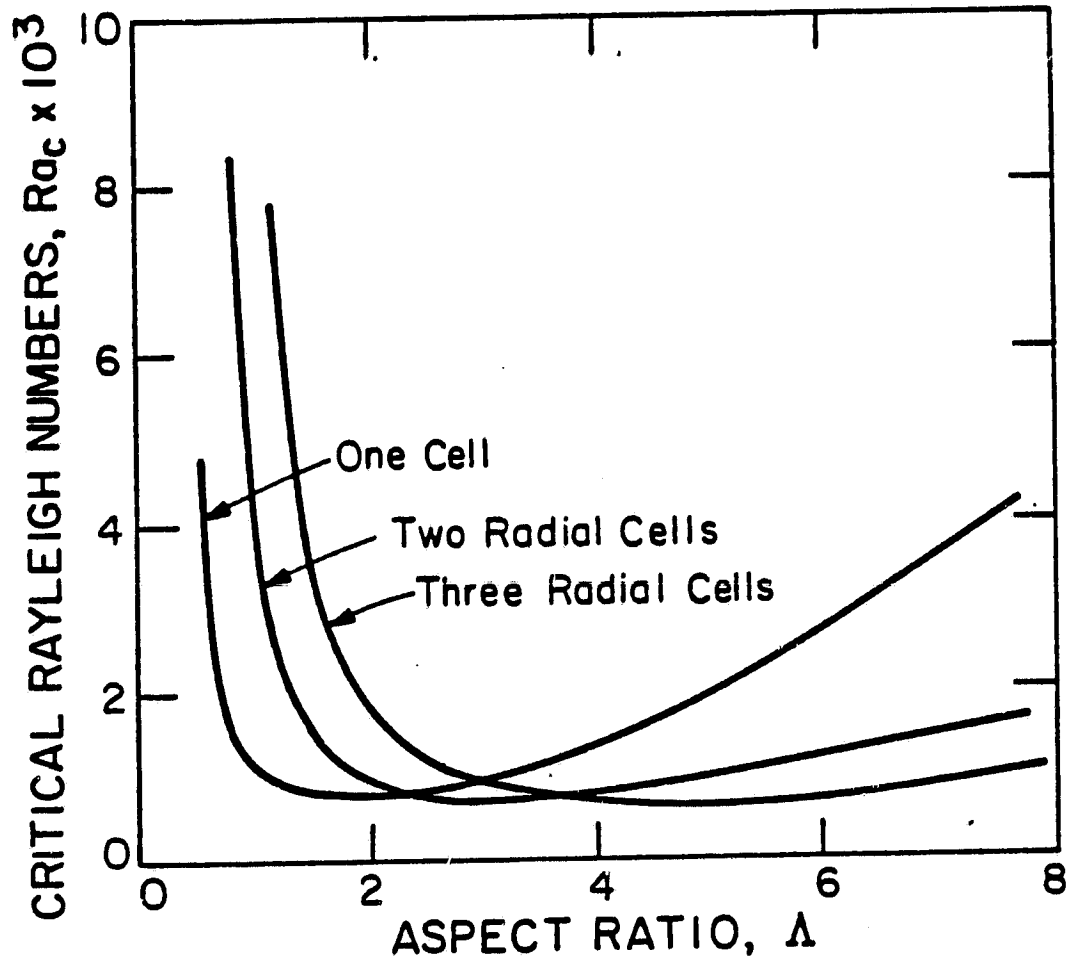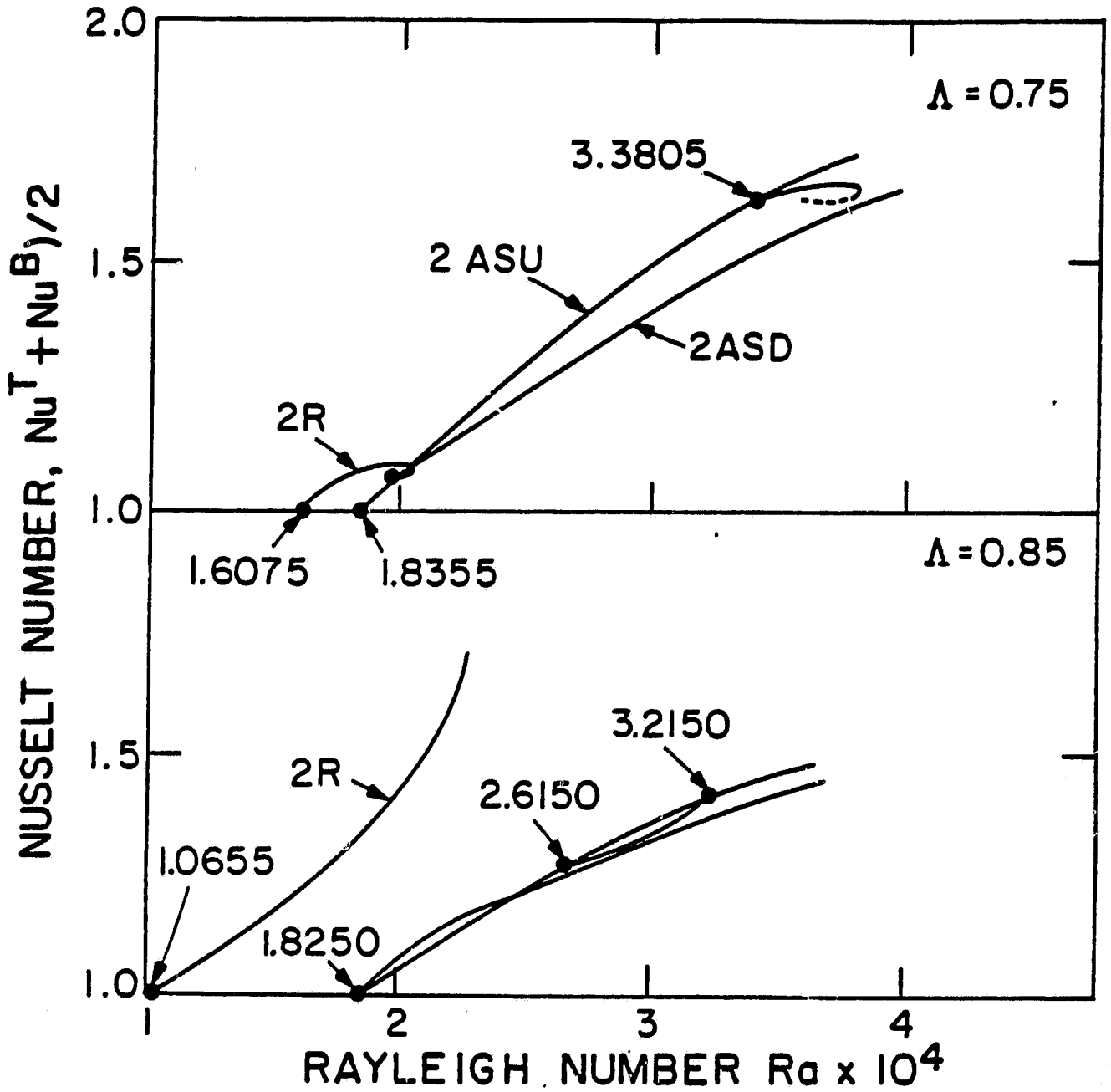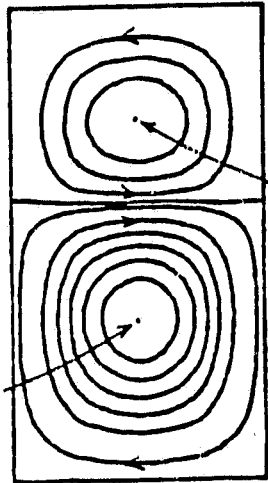
Figure 1
Yamaguchi et al.
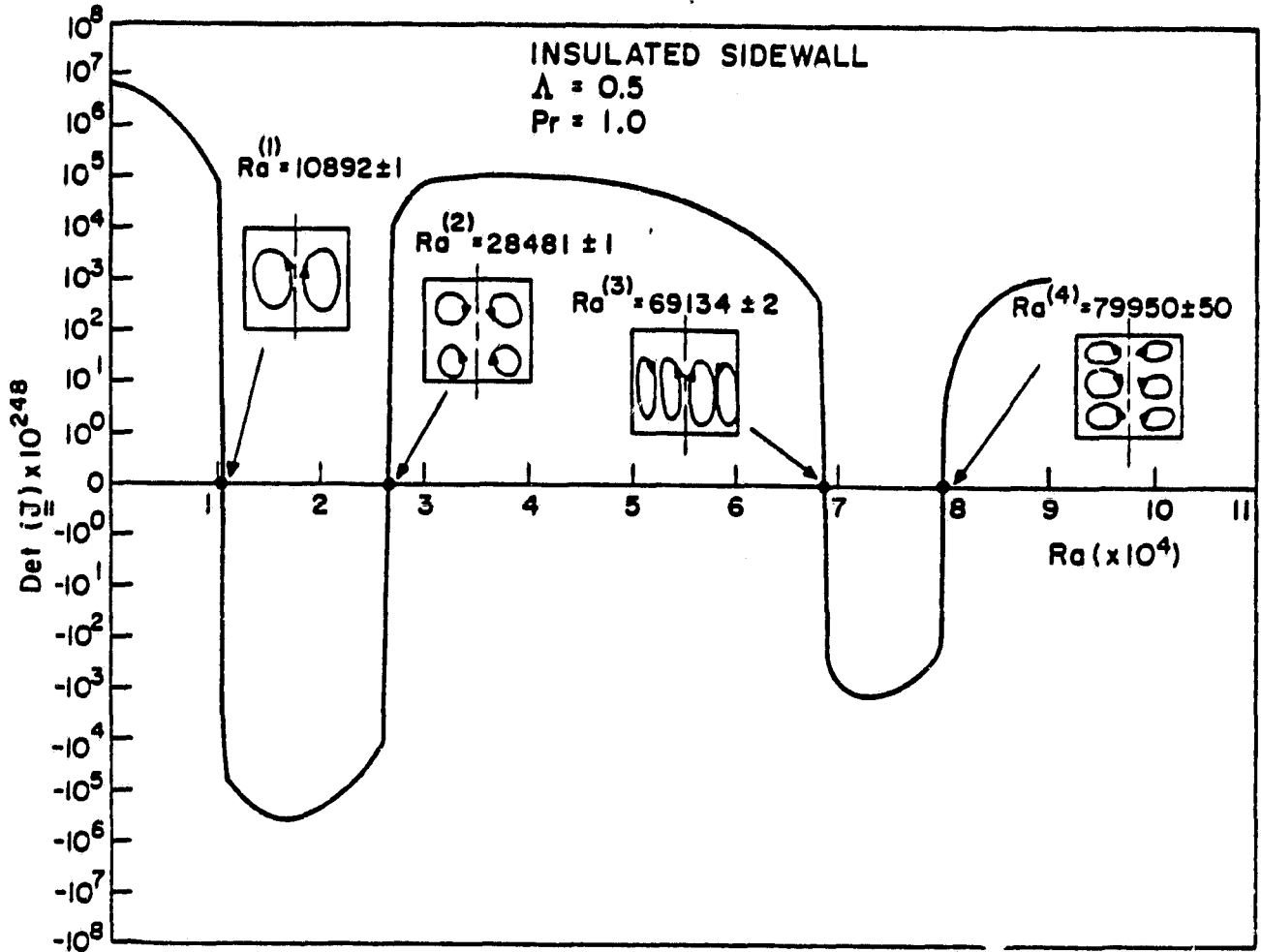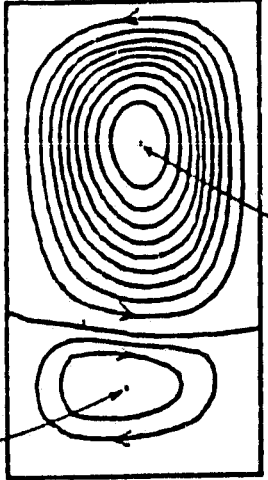
Figure 2

Yamaguchi et al.

INSULATED SIDE WALL

$\Lambda \equiv R/H$

[2R2A]

[2A]

[3R]

[2R]

[1]

[1R]

[3R]

[2R]

[2R]

[2R]

[1R]

[3R]

[4R]

[2R]

[3R]

ASPECT RATIO Λ

CRITICAL RAYLEIGH NUMBER $Ra_c \times 10^3$

Figure 3

Yamaguchi et al.
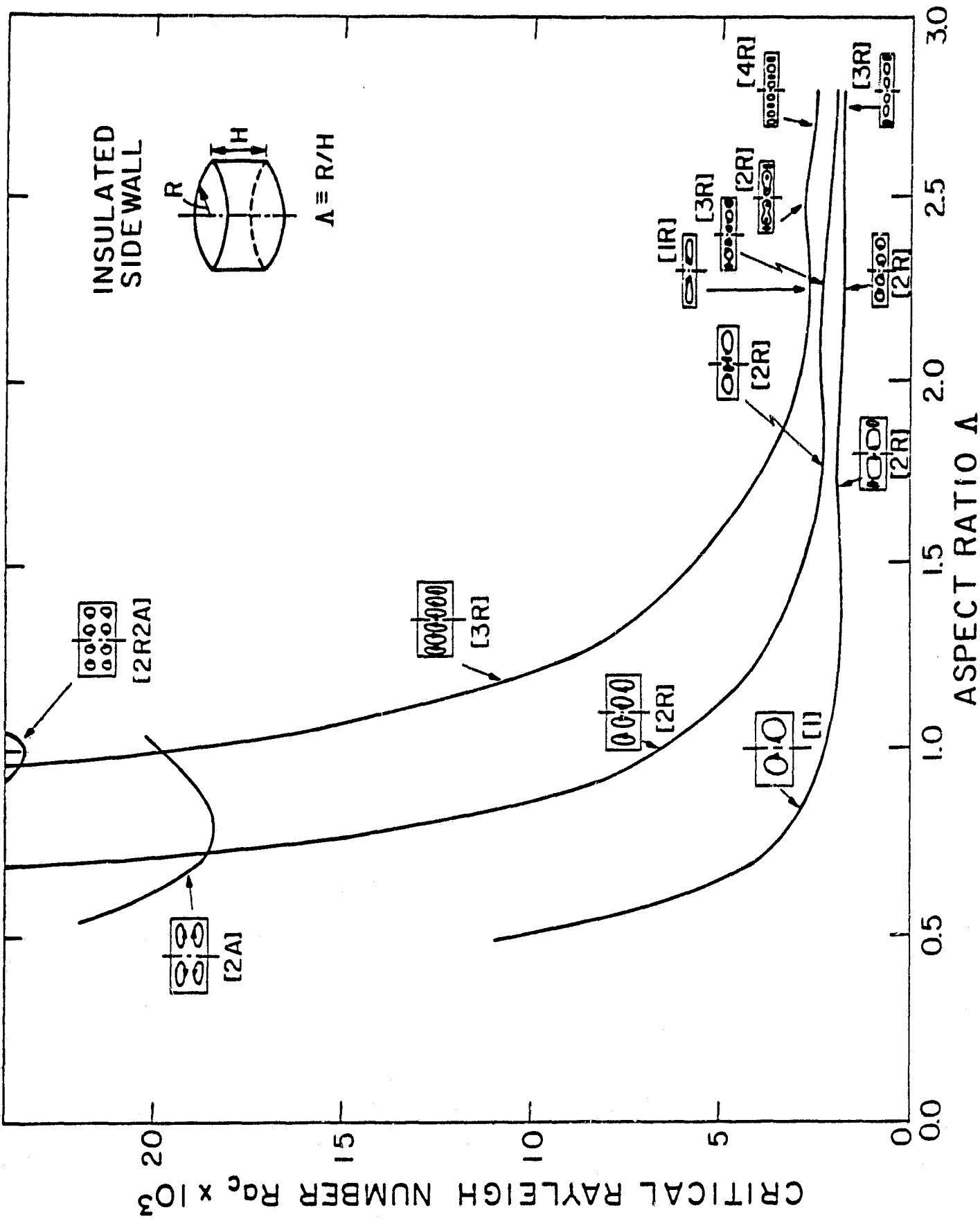
$\Lambda = 0.50$

$Ra_c^{(1)} = 10,892$

$\Lambda = 0.75$

$Ra_c^{(1)} = 3,450$

$\Lambda = 1.00$
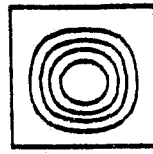
$Ra_c^{(1)} = 2,270$

$\Lambda = 1.70$
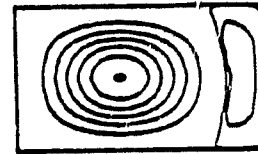
$Ra_c^{(1)} = 1,956$

$Ra_c^{(2)} = 28,410$

$Ra_c^{(2)} = 16,080$
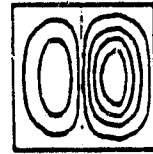
$Ra_c^{(2)} = 6,678$
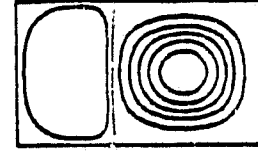
$Ra_c^{(2)} = 2,312$

$Ra_c^{(3)} = 69,134$

$Ra_c^{(3)} = 18,360$

$Ra_c^{(3)} = 20,610$
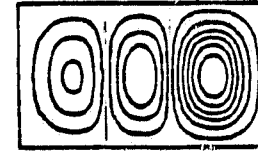
$Ra_c^{(3)} = 4,076$

$\Lambda = 2.00$
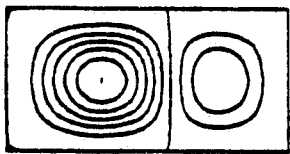
$Ra_c^{(1)} = 1,871$

$\Lambda = 2.25$
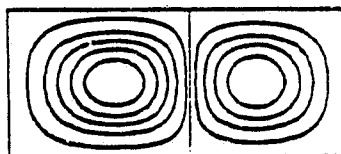
$Ra_c^{(1)} = 1,800$

$\Lambda = 2.50$
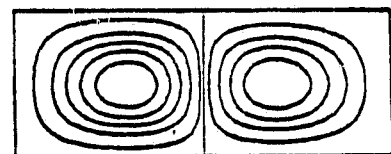
$Ra_c^{(1)} = 1,720$
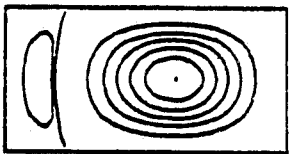
$Ra_c^{(2)} = 2,344$
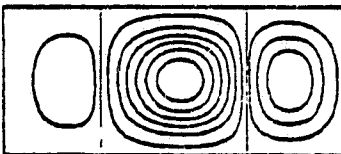
$Ra_c^{(2)} = 2,322$
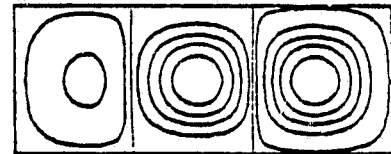
$Ra_c^{(2)} = 2,060$
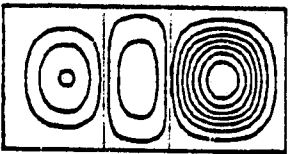
$Ra_c^{(3)} = 2,951$
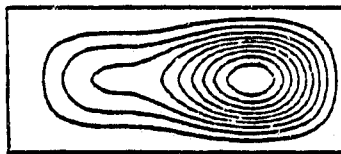
$Ra_c^{(3)} = 2,744$
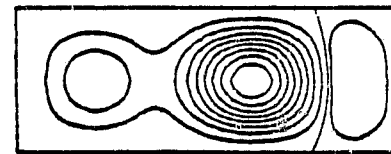
$Ra_c^{(3)} = 2,840$

Figure 5

Yamaguchi et al

Ra = 2.9 x 10⁴

θ

$\psi = -0.2794$

$\psi = 4.699$

Ra = 2.5 x 10⁴

θ

$\psi = -0.0740$

$\psi = 4.954$

Ra = 1.0 x 10⁴

θ

$\psi = 3.183$

Ra = 2.312 x 10³

$\theta = 0$

$\theta = 1$

Figure 6. Yamaguchi et al.

$Ra = 2.9 \times 10^4$

θ

$\psi = -0.3035$

$\psi = 4.635$

$Ra = 2.0 \times 10^4$

θ

$\psi = -0.7213$

$\psi = 2.436$

$Ra = 1.0 \times 10^4$

θ

$\psi = -0.5068$

$\psi = 0.9412$

$Ra = 6.519 \times 10^3$

$t = 0$

$\theta = 1$

$\theta = 1$
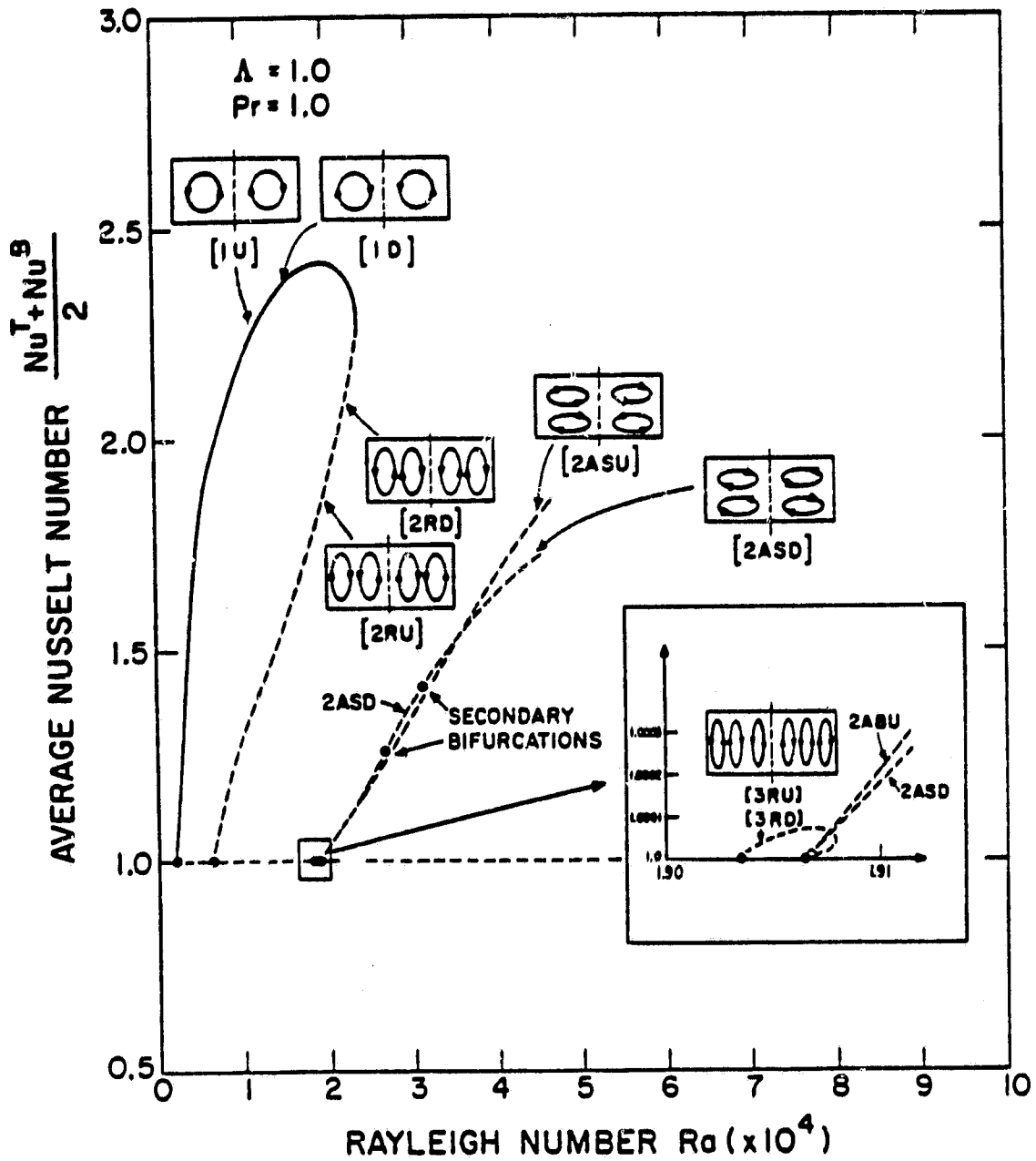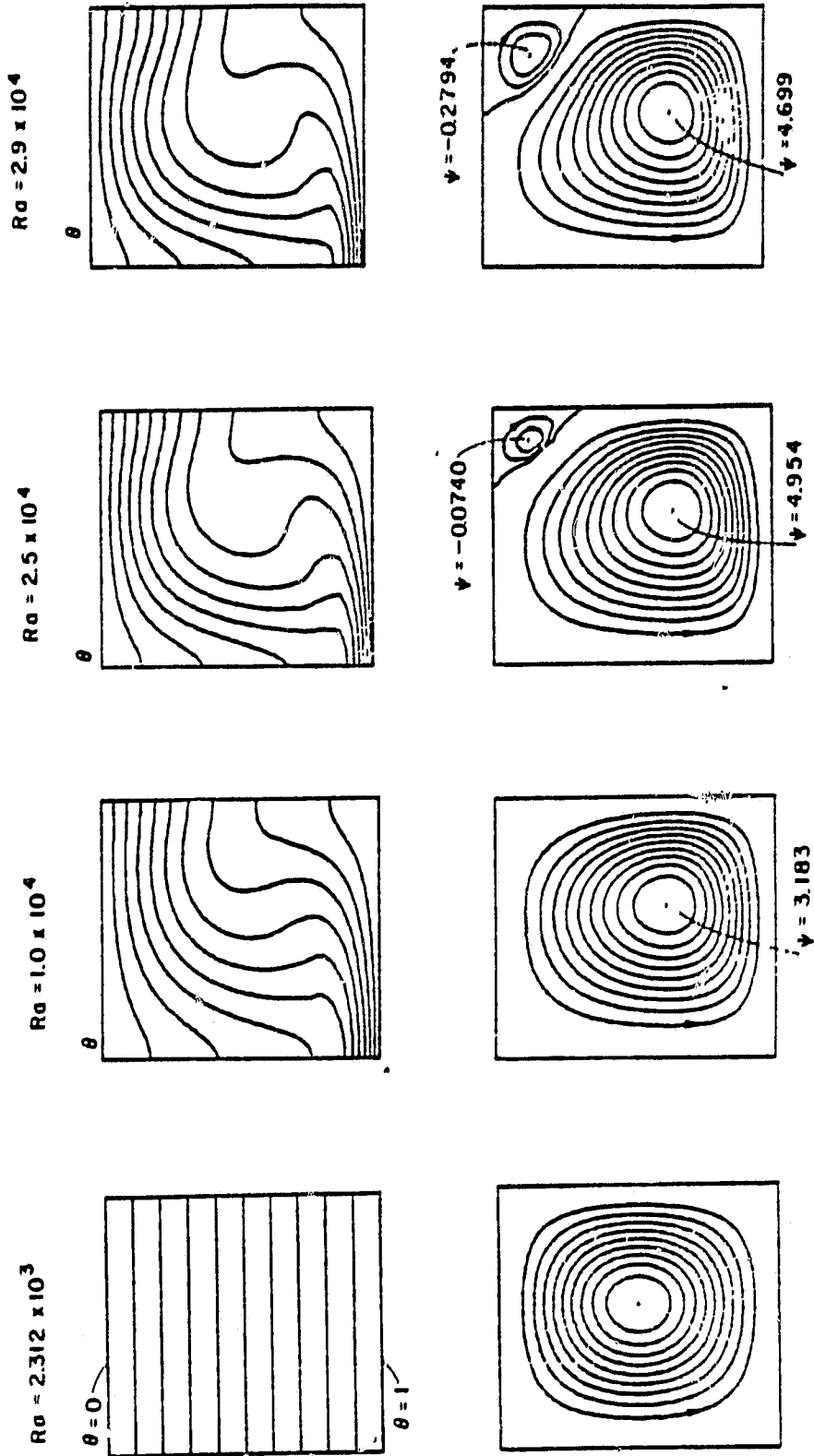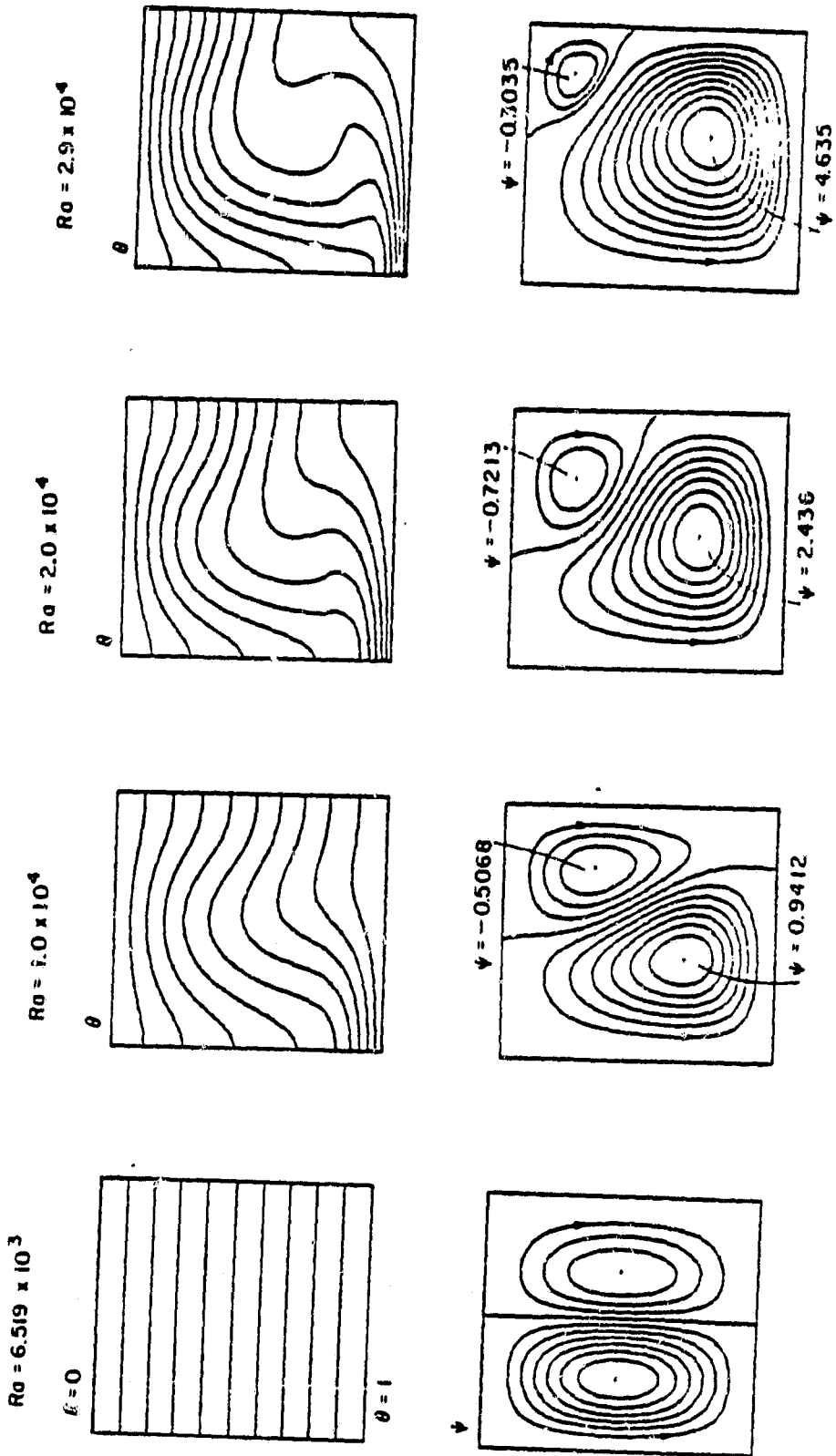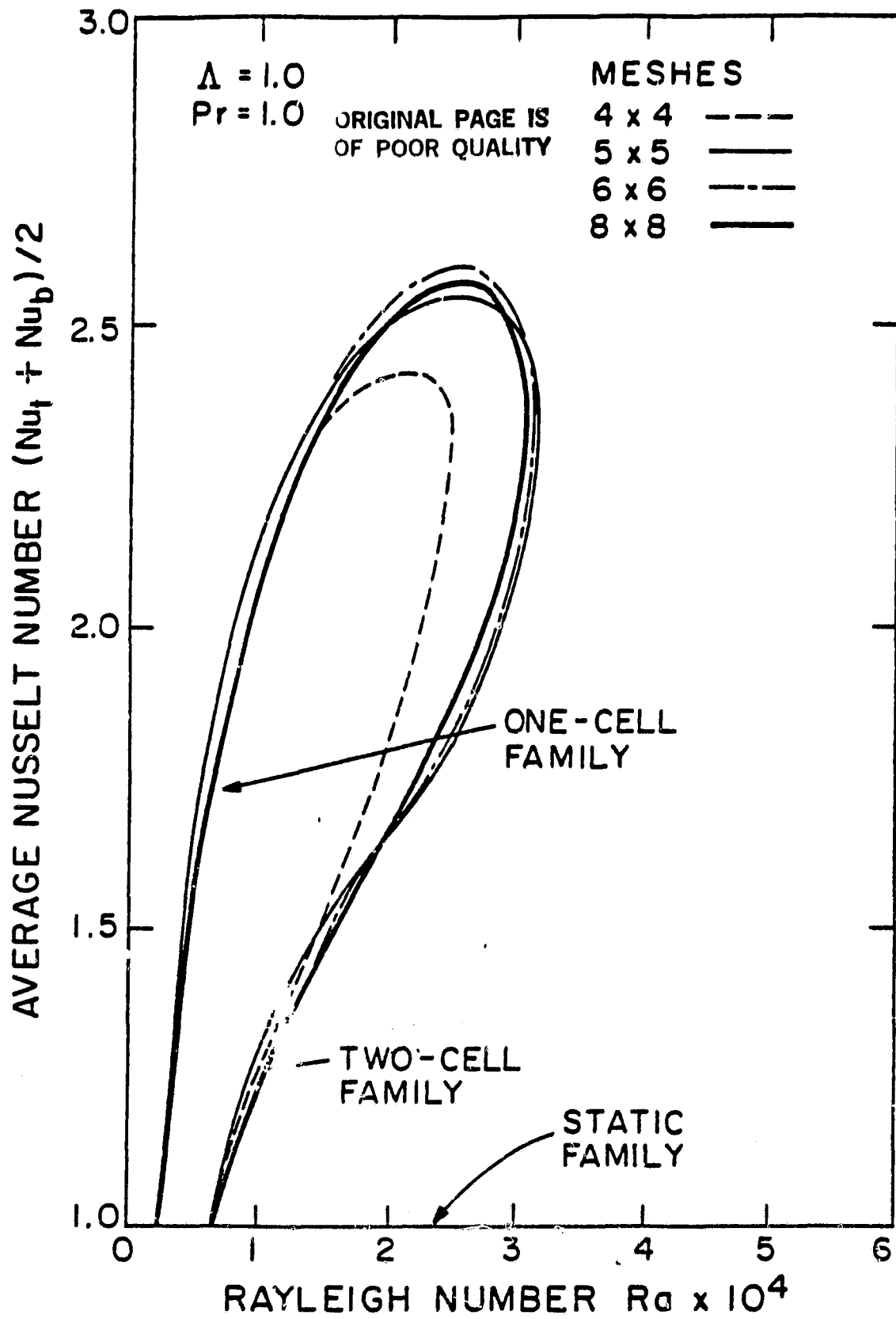
iamaguchi et al.

Figure 8.

Yamaguchi et al.
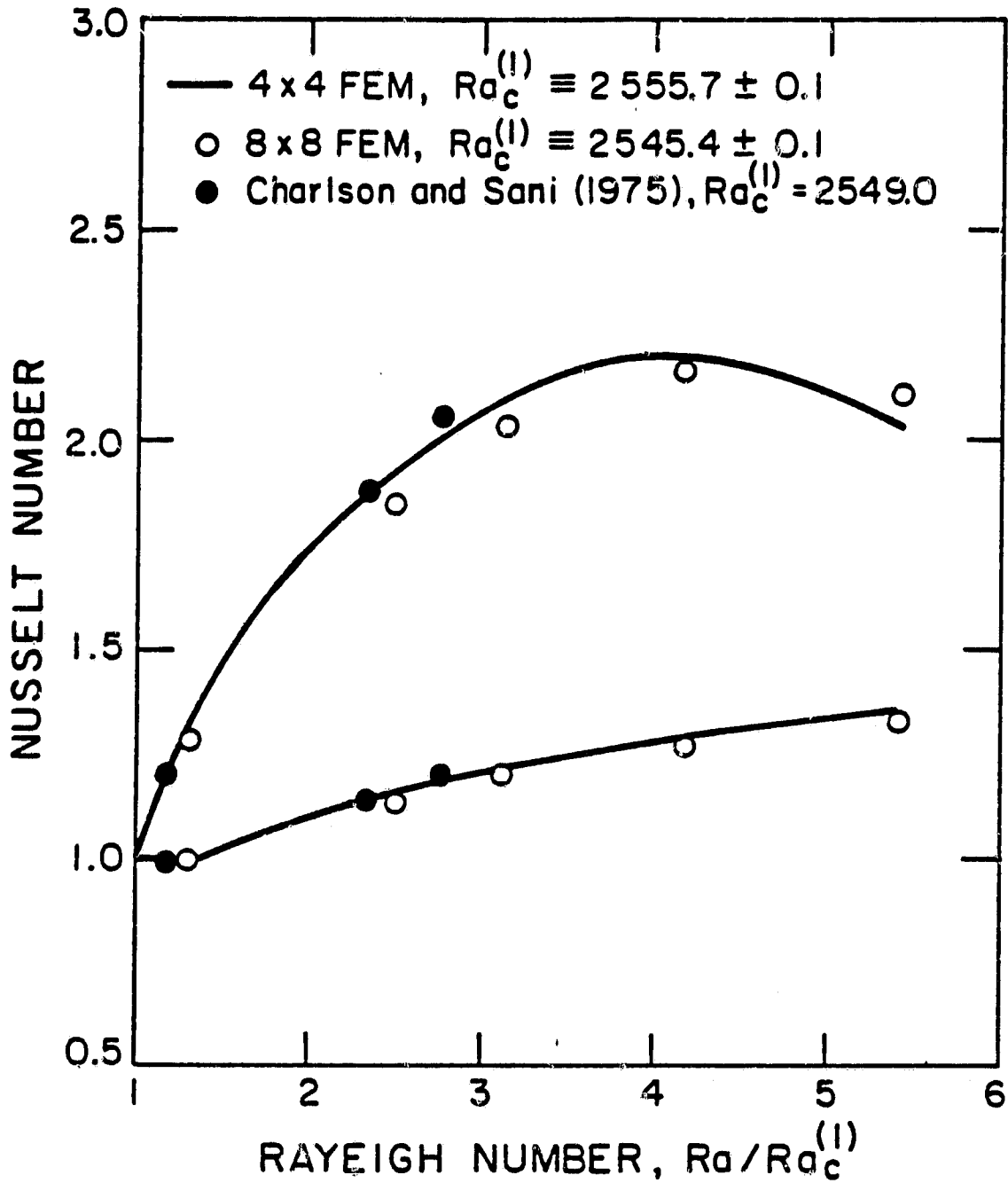
Figure 9
Yamaguchi et al.
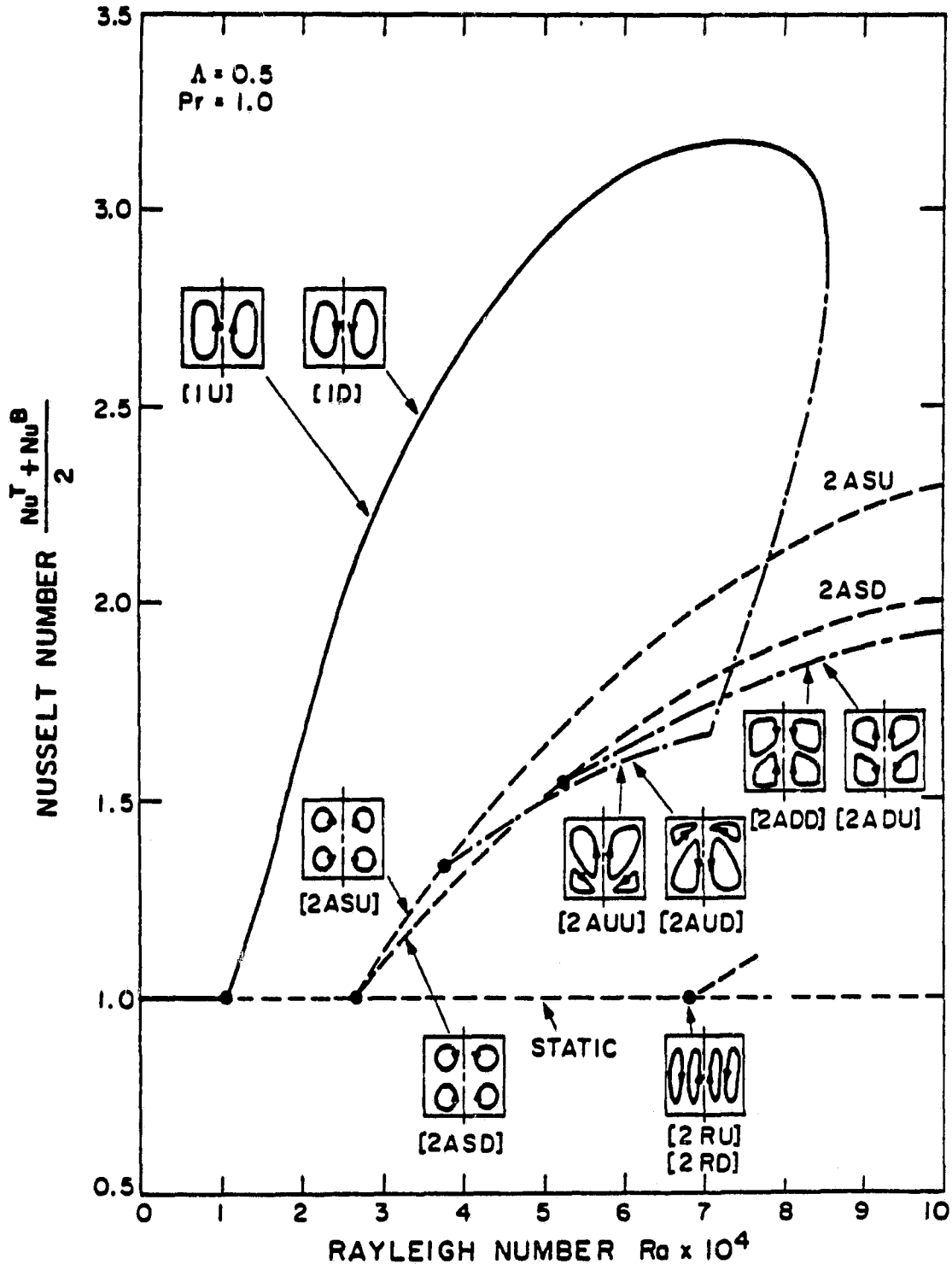
Figure 10

Yamaguchi et al.
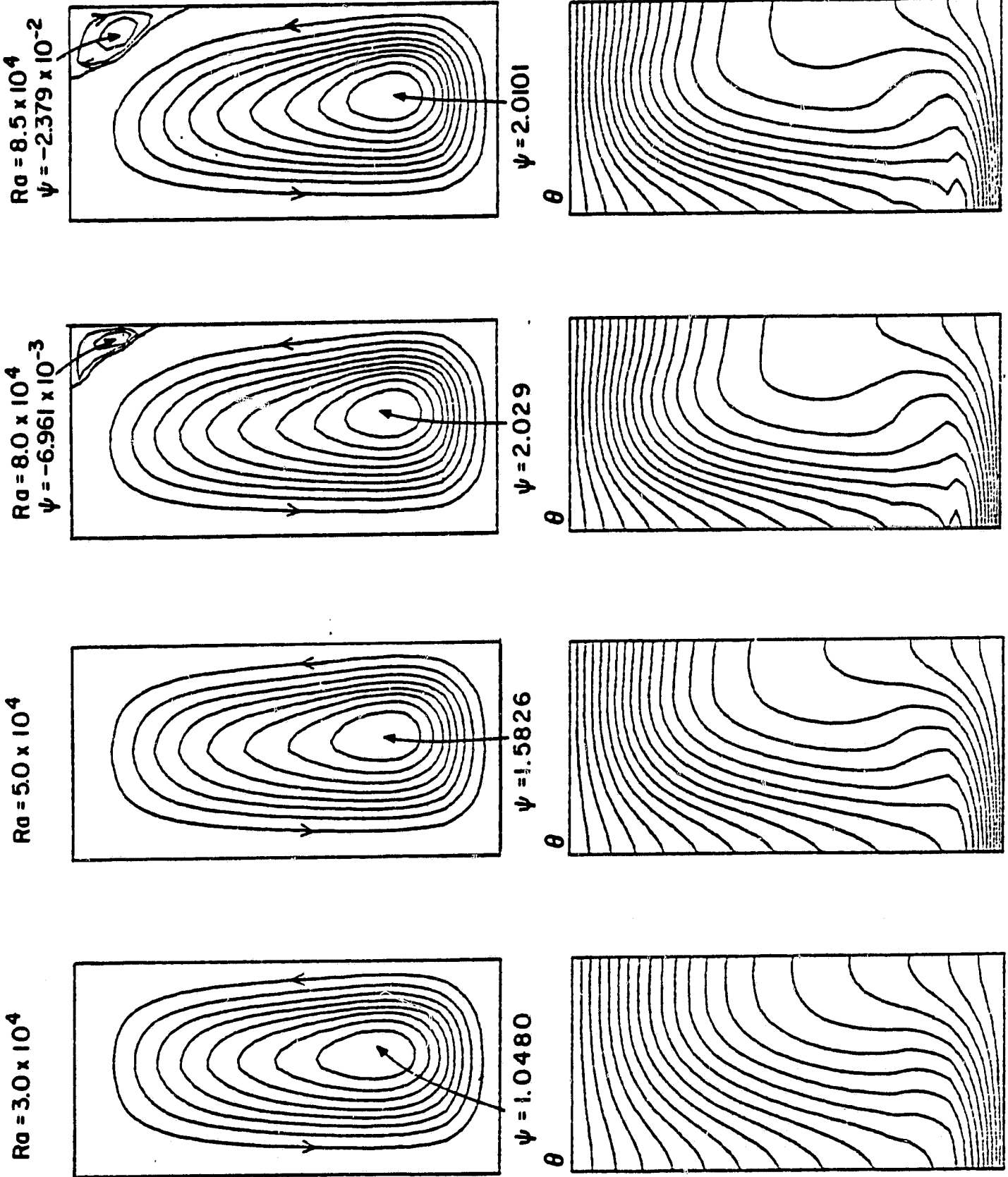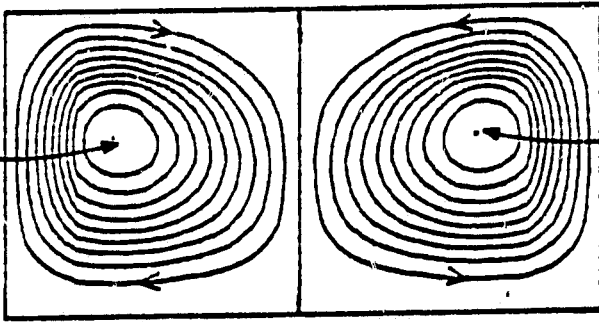
$Ra = 8.5 \times 10^4$
$\psi = -2.379 \times 10^{-2}$
$\psi = 2.0101$

$Ra = 8.0 \times 10^4$
$\psi = -6.961 \times 10^{-3}$
$\psi = 2.029$
$\psi = 2.001$

$Ra = 5.0 \times 10^4$
$\psi = 1.5826$

$Ra = 3.0 \times 10^4$
$\psi = 1.0480$

θ

Figure 11. Yamaguchi et al.

Ra = 2.5 x 10^5
$\psi = -2.119$

$\psi = 2.119$

θ

Ra = 1.0 x 10^5
$\psi = -1.322$

$\psi = 1.322$

θ

Ra = 3.0 x 10^4
$\psi = -2.321 \times 10^{-1}$

$\psi = 2.321 \times 10^{-1}$

θ

Ra = 2.65 x 10^4
$\psi = -2.485 \times 10^{-2}$

$\psi = 2.485 \times 10^{-2}$

θ

Ra = 8.5 x 10^4
ψ = -6.937 x 10^{-2}

ψ = 1.872

θ

Ra = 7.7 x 10^4
ψ = -1.953 x 10^{-1}

ψ = 1.415

θ

Ra = 5.0 x 10^4
ψ = -2.742 x 10^{-1}

ψ = 8.425 x 10^{-1}

θ

Ra = 4.0 x 10^4
ψ = -3.399 x 10^{-1}

ψ = 5.928 x 10^{-1}

θ
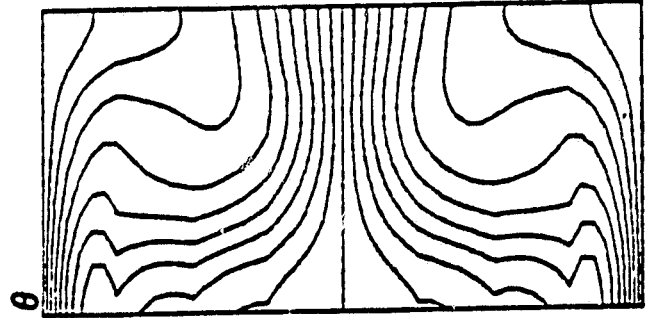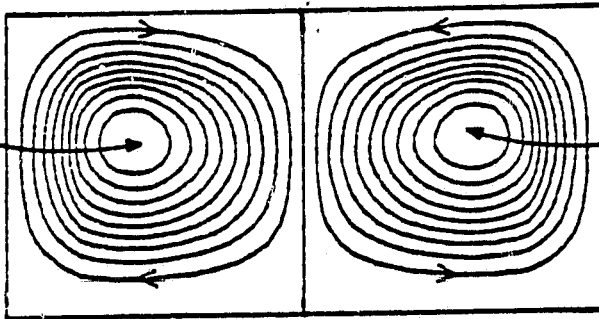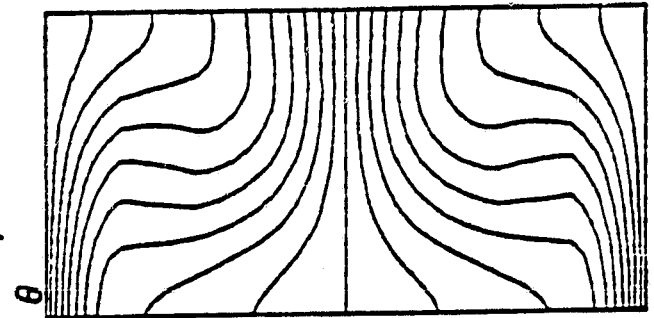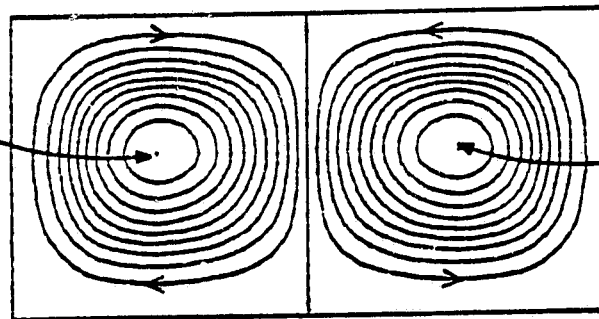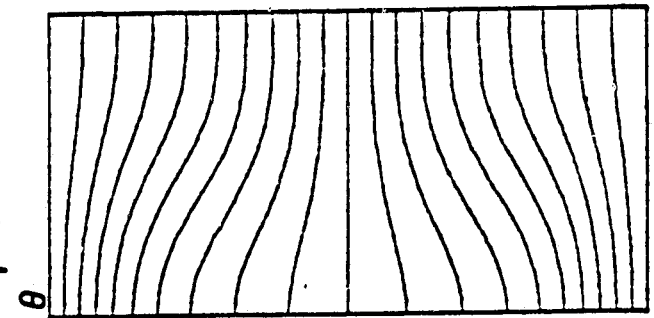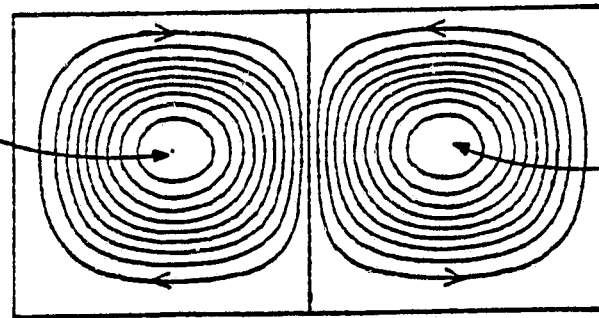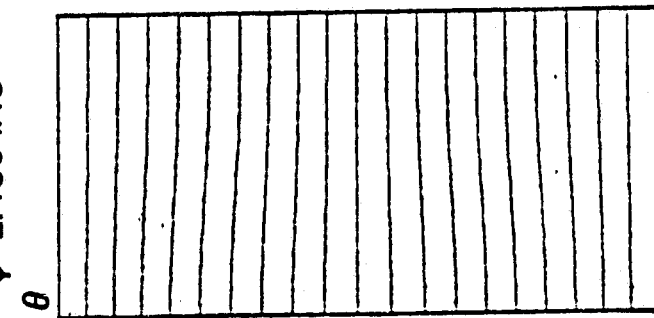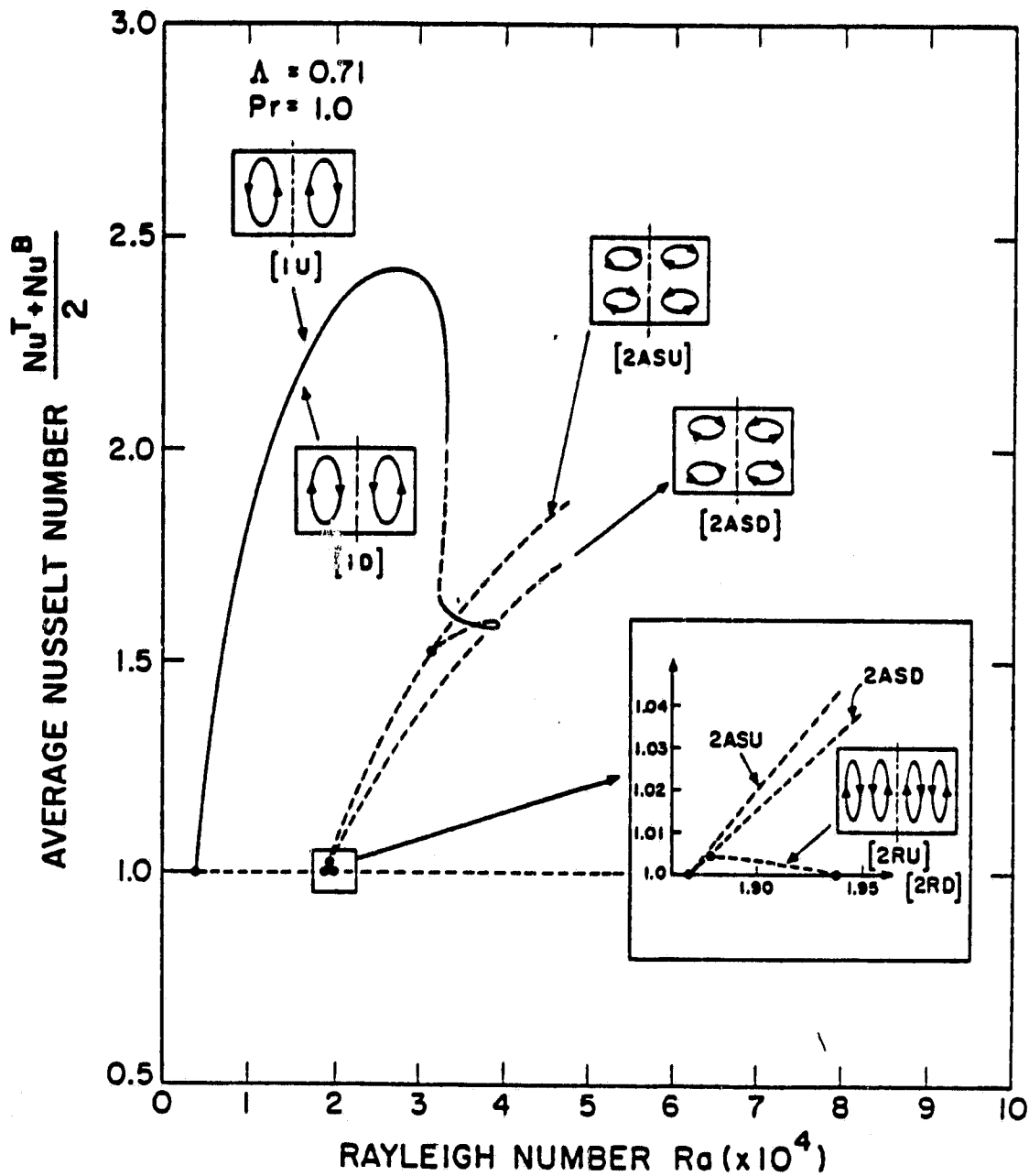
Fig. 13. Yamauchi et al.

Fig. 14
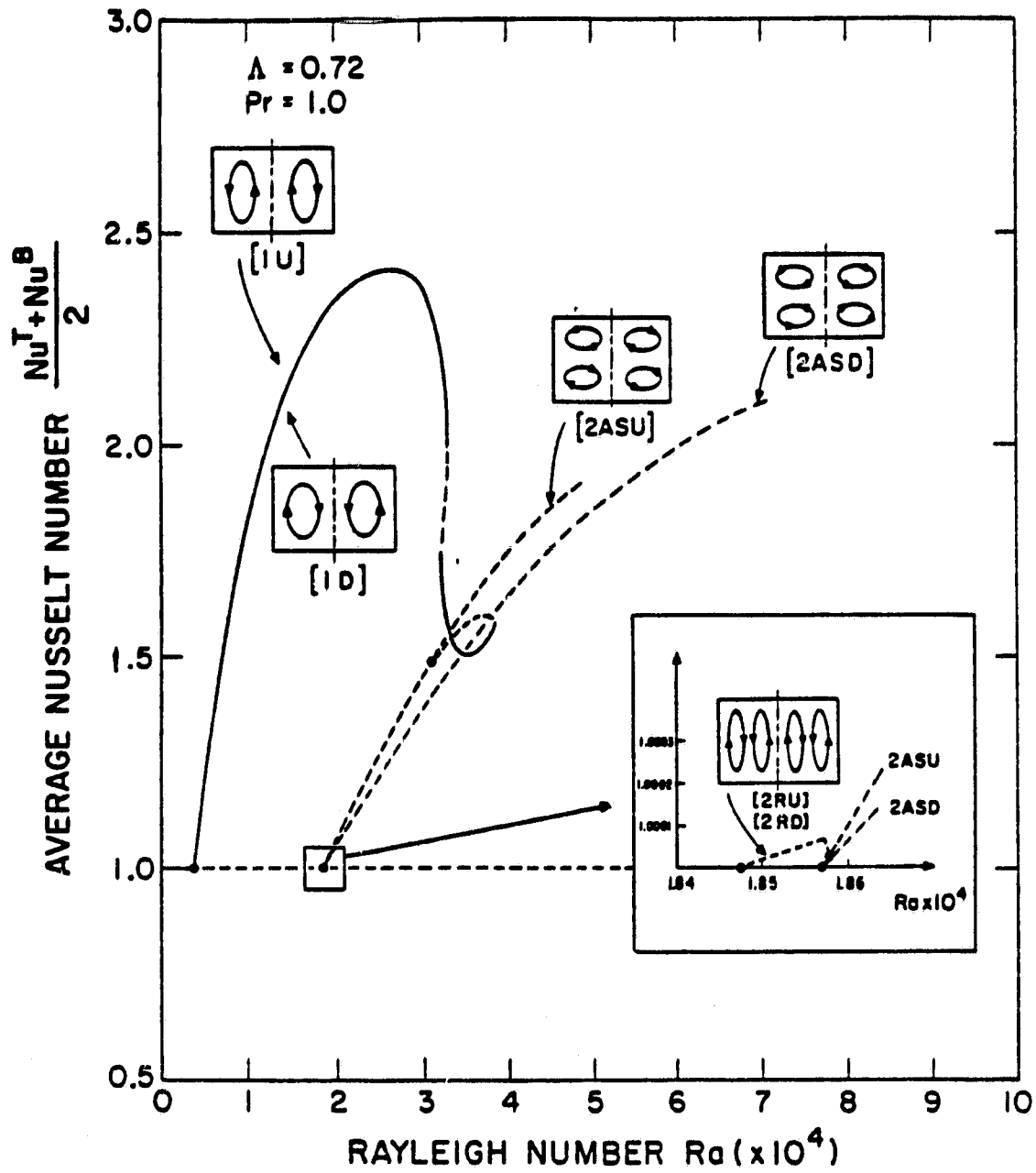
Yamaguchi et al.

Fig. 15

Yamaguchi et al
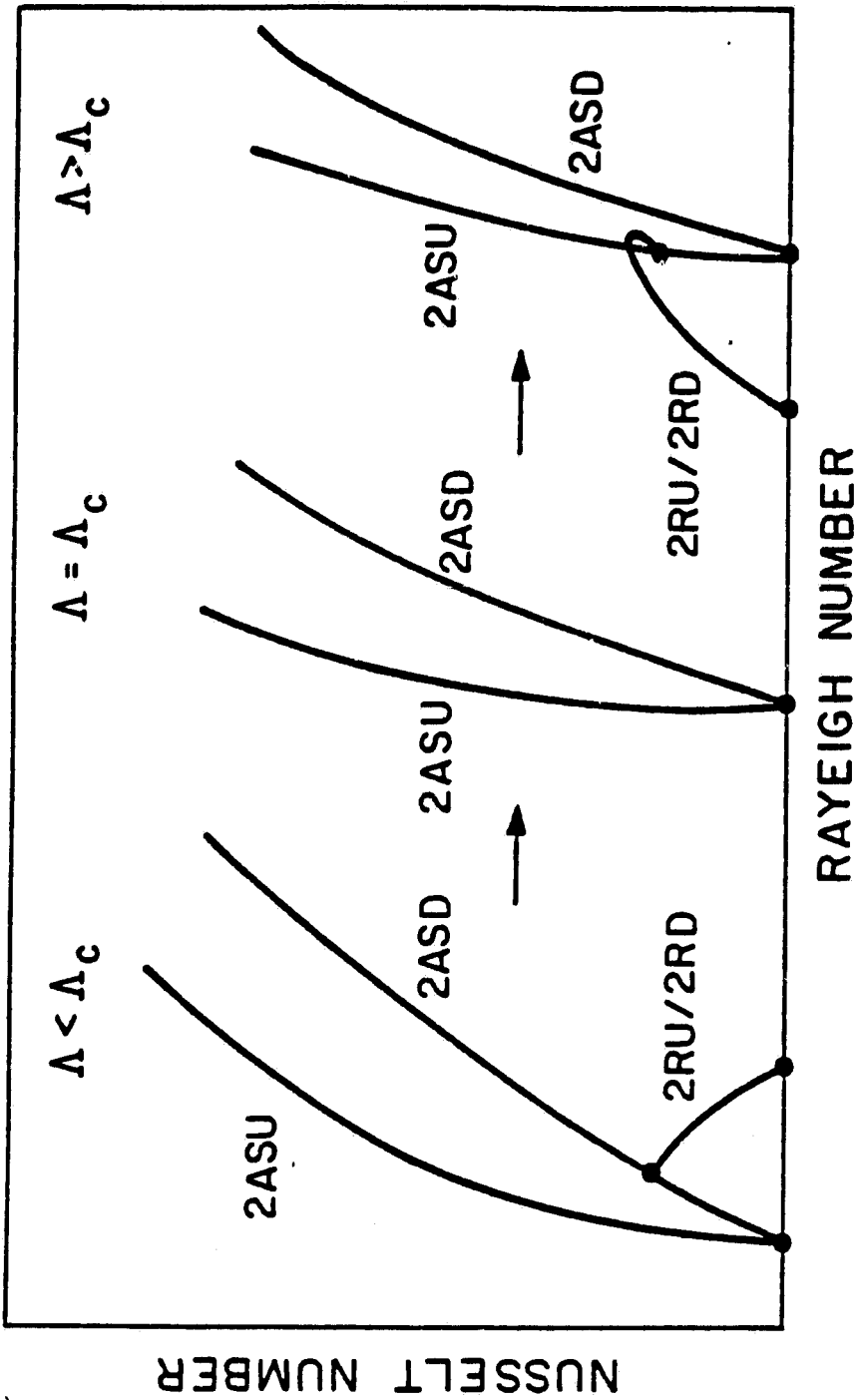
Figure 16
Yamaguchi et al.

Figure 17
Yamaguchi et al.

RAYLEIGH NUMBER

NUSSELT NUMBER

$\Lambda > \Lambda^*$

$\Lambda = \Lambda^*$

MULTIPLE-LIMIT-POINT

$\Lambda < \Lambda^*$

2ASU

2RU/2RD

1U/1D
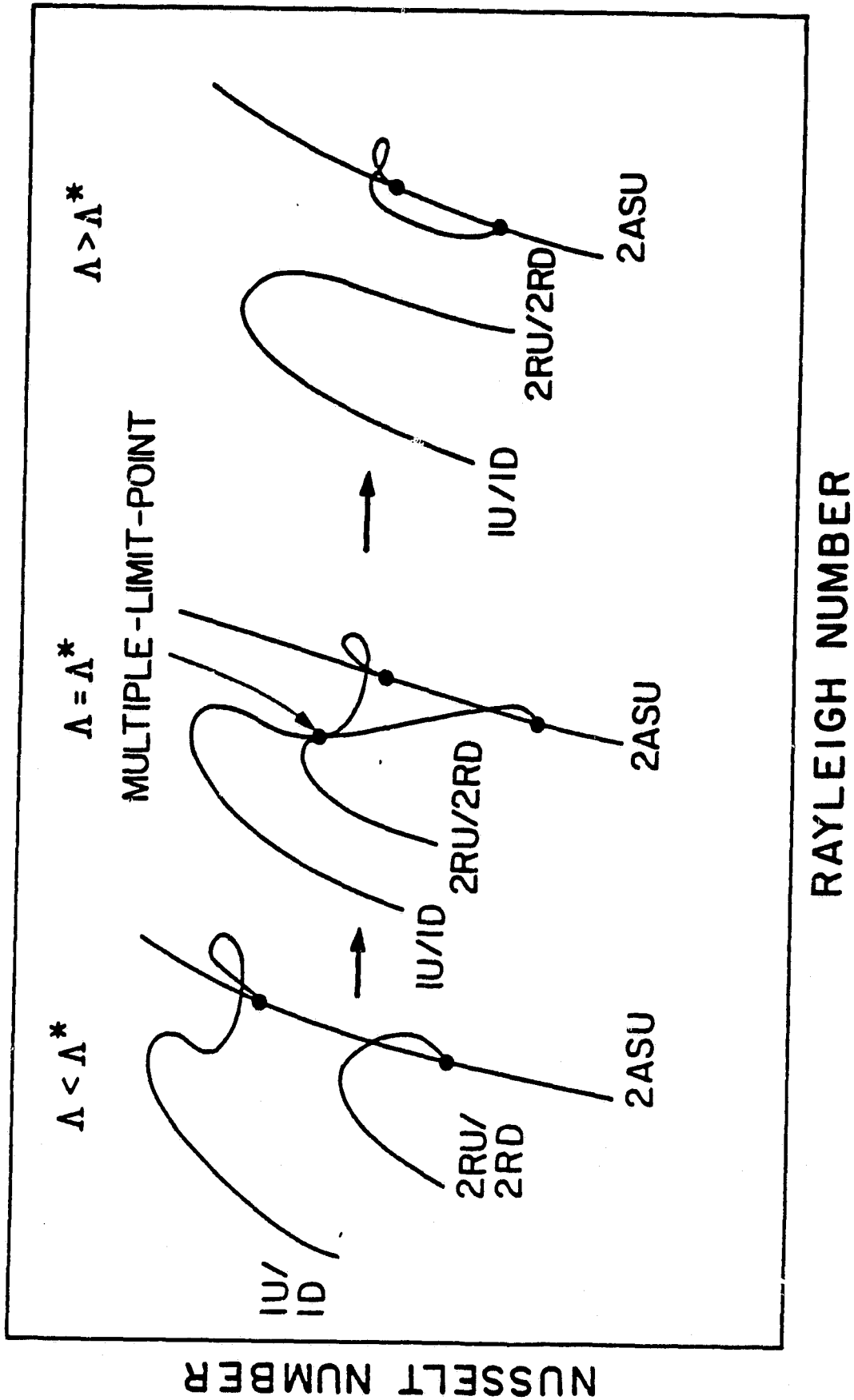
Figure 18   Yamaguchi et al.
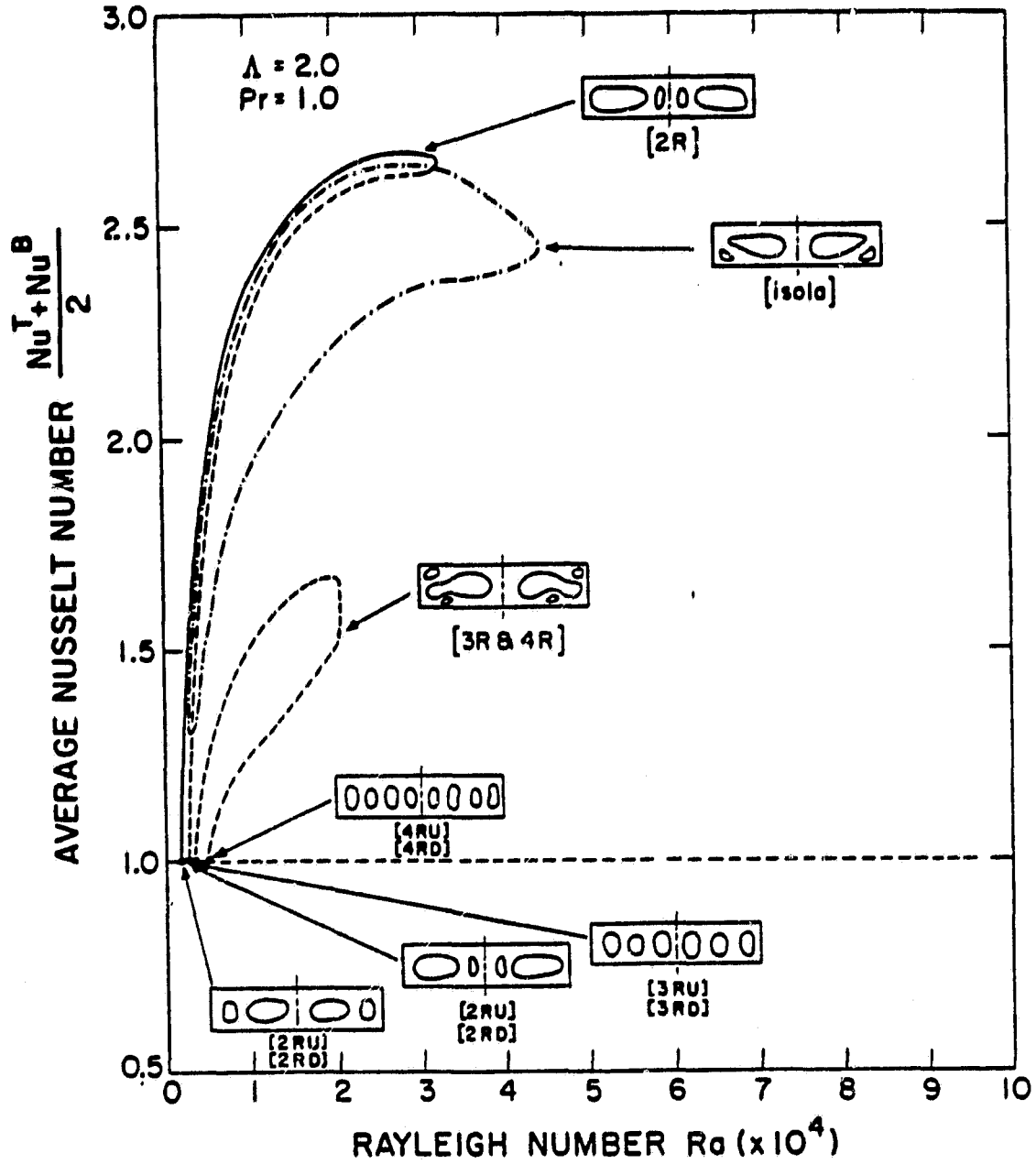
Figure 19

FIRST 2RU FAMILY

(a) Ra = 1.8 x 10^3
ψ = -0.06
ψ = 0.04

(b) Ra = 1.0 x 10^4
ψ = -1.35
ψ = 10.94
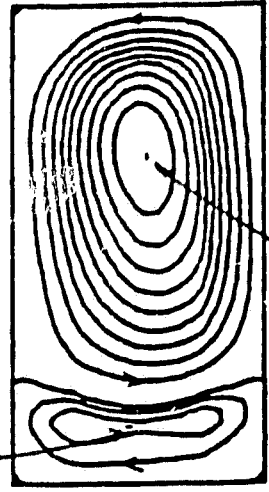
(c) Ra = 3.2 x 10^4
ψ = -0.18
ψ = 17.70

SECOND 2RU FAMILY

(d) Ra = 2.3 x 10^3
ψ = -.003
ψ = 0.24

(e) Ra = 1.0 x 10^4
ψ = -0.22
ψ = 10.87

(f) Ra = 3.0 x 10^4
ψ = -0.63
ψ = 17.40
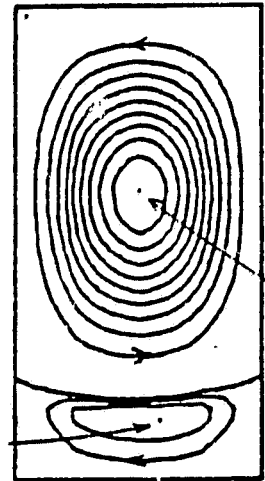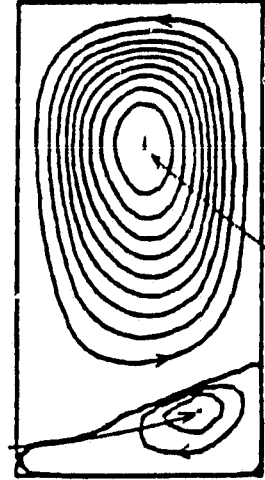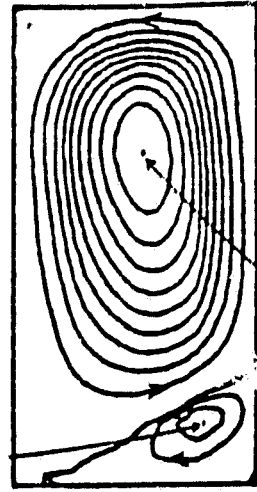
Figure

TOP OF ISOLA

(a) Ra = 3.01 × 10³
$\psi = -2.99$
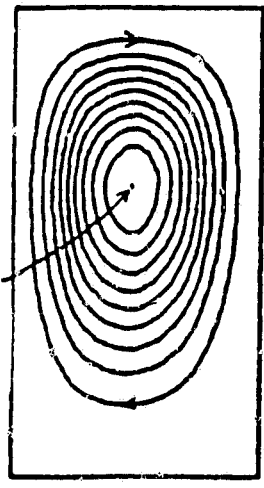
(b) Ra = 1.5 × 10⁴
$\psi = -13.38$
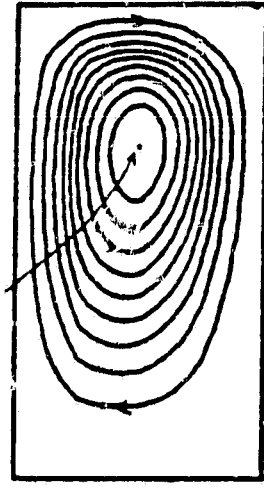
(c) Ra = 4.4 × 10⁴
$\psi = -17.67$
$\psi = 0.83$
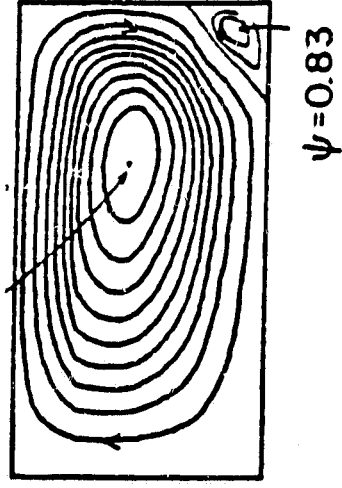
BOTTOM OF ISOLA

(d) Ra = 3.05 × 10³
$\psi = -2.86$

(e) Ra = 3.5 × 10³
$\psi = -3.20$
$\psi = 0.07$

(f) Ra = 1.0 × 10⁴
$\psi = -8.16$
$\psi = 1.25$

Yamaguchi et al.

Figure 21

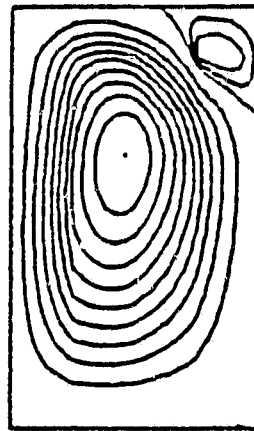$\Lambda = 1.4$

$\Lambda = 1.4$

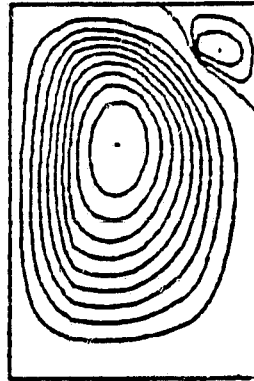$Ra = 1.0 \times 10^4$

$\Lambda = 1.6$

$Ra = 4.0 \times 10^4$

$\Lambda = 1.6$

$\Lambda = 1.8$

$\Lambda = 1.8$

Yamaguchi et al.
Figure 22